Carbon 119 (2017) 403–418

Contents lists available at ScienceDirect

Carbon

journal homepage: www.elsevier.com/locate/carbon

# Significant effect of sorbed water on the electrical and dielectric behavior of graphite oxide

Xinghua Hong [a, b], Weidong Yu [b], D.D.L. Chung [a, *]

[a] Composite Materials Research Laboratory, Department of Mechanical and Aerospace Engineering, University at Buffalo, The State University of New York, Buffalo, NY 14260-4400, USA
[b] Key Laboratory of Textile Science & Technology, Ministry of Education, College of Textiles, Donghua University, Shanghai, 201620, China

ARTICLE INFO

*Article history:*
Received 2 November 2016
Received in revised form
2 April 2017
Accepted 8 April 2017

ABSTRACT

This paper reports the unexpectedly strong effect of 4 wt% additional sorbed water on the electrical and dielectric properties (50 Hz–2 MHz) of graphite oxide (GO) containing 18 wt% sorbed water. Water contents of 18 and 22 wt% (designated $GO_{18}$ and $GO_{22}$, respectively) are compared, with the former obtained by heating at 60 °C (3 h) immediately before testing. The additional water increases the conductivity and decreases the conductivity anisotropy. It enhances the conductivity at any frequency, but enhances the relative dielectric constant (real part) at <200 Hz. Above 200 Hz, it decreases the dielectric constant. Concerning the specimen-contact interface, the interfacial resistivity and specific interfacial capacitance are decreased. The negative of the relative dielectric constant (imaginary part) is greatly increased by the additional water. Reduced graphite oxide (RGO) exhibits higher conductivity than $GO_{22}$, which exhibits much higher conductivity than $GO_{18}$. Compared to RGO, $GO_{22}$ exhibits lower conductivity, higher interfacial resistivity and higher specific interfacial capacitance. The relative dielectric constant (real part) is higher for $GO_{22}$ than RGO at <500 Hz (due to the water), but is lower for $GO_{22}$ at >500 Hz. The through-thickness electrical/dielectric properties of $GO_{22}$ are modeled with $GO_{18}$, additional water and air in parallel.



## 1. Introduction

### 1.1. Graphite oxide

Graphite oxide (GO) is widely used as a precursor for graphene. The GO is attractive for humidity sensing (with fast response), due to an increase in humidity causing the impedance to decrease [1] and the capacitance to decrease [2]. Furthermore, GO is attractive for filtration and separation, due to it very high water permeability compared to the permeability of other species [3]. Other potential applications of GO include ammonia gas sensor, transparent conductors, transistors, field emitters, photovoltaics and memory devices [4–6].

In contrast to graphite, GO is hydrophilic, due to the abundance of oxygen-containing functional groups (as shown by infrared spectroscopy [7]). Thus, GO absorbs and adsorbs water, as shown by the increase in the interlayer spacing [8,9]. The sorbed water includes intercalated interlayer water and water in the void between the grains [9]. For GO containing 15–27 wt% sorbed water, the sorbed water is mainly interlayer water [9].

Partly due to the ionic conductivity of water, the sorbed water greatly increases the conductivity of the GO [7,10,11]. Moreover, the sorbed water reacts with the surface functional groups of GO to form $H^+$ ions (protons), which contribute to increasing the conductivity [1]. The GO with absorbed/adsorbed water is a mixed conductor with ionic (proton) conductivity and electronic conductivity. In case that the sorbed water content is high enough for the proton conductivity to dominate, the material has a potential application as an electrolyte in electrochemical devices, such as a proton conducting membrane in a fuel cell [11].

The electrical and dielectric properties are key to the use of materials in electronic, ferroelectric and electrochemical devices. In particular, the dielectric properties are relevant to the interactions of materials with electromagnetic radiation. Such interactions occur in electromagnetic interference shielding, low observability, radar-based monitoring, and radio-frequency identification.

Prior reports of the effect of sorbed water on the electrical and

* Corresponding author.
*E-mail address:* ddlchung@buffalo.edu (D.D.L. Chung).
*URL:* http://alum.mit.edu/www/ddlchung

http://dx.doi.org/10.1016/j.carbon.2017.04.012
0008-6223/

dielectric behavior of GO includes the following. Increase of the relative humidity from 30% to 100% causes the conductivity to increase from $10^{-6}$ to $10^{-2}$ S/cm [10]. Increase in the relative humidity from 40% to 100%, increases the conductivity from $7 \times 10^{-3}$ S/m to $2 \times 10^{-2}$ S/m, but decreases the relative dielectric constant (assumed to be independent of the frequency in the analysis) from 100 to 8 [11]. The through-thickness conductivity of GO containing 16 wt% sorbed water is $10^{-3}$ S/m [12]. The in-plane conductivity of GO increases with increasing humidity, such that the contribution to the measured resistance of the interface (between the GO specimen and an electrical contact) increases with increasing humidity [1]. The rotation of the confined water molecules affects the dielectric behavior [9]. In spite of the above findings, the effect of sorbed water on the electrical and dielectric behavior has not been adequately investigated in the prior work.

Since sorbed water is naturally present in GO that has been exposed to room atmosphere, GO that contains sorbed water is commonly used in practice. Therefore, it is important to study the effect of sorbed water on the electrical and dielectric behavior of GO.

### 1.2. Methodology of electrical and dielectric testing

The dielectric behavior of a material is described by the real and imaginary parts of the relative dielectric constant (also known as the relative permittivity). The real part is often simply referred to as the relative dielectric constant. The real part relates to the polarization behavior (which in turn relates to the capacitance), whereas the imaginary part relates to the energy loss, which can be due to the conduction loss and dielectric loss. In case of a material that has substantial conductivity, the conduction loss dominates the energy loss. Due to the fact that an RLC meter (as commonly used for studying the dielectric behavior of materials [10]) is not meant for measuring the capacitance of a material of low resistance, the measurement of the relative dielectric constant (both the real and imaginary parts, which are related) of a conductive material can be reliably performed using an RLC meter, only if an electrically insulating film is positioned between the specimen and an electrical contact. On the other hand, the presence of this insulating film greatly increases the resistance of the system, thereby making it not possible to measure the conductivity of the specimen and causing the measured imaginary part of the relative dielectric constant to reflect the dielectric loss and not the conduction loss. For a material with the loss dominated by conduction loss, this experimental condition results in a value of the imaginary part of the relative dielectric constant that is much lower than the true value.

Due to the issues mentioned above, a material of substantial conductivity should be tested in the presence of an insulating film when the relative dielectric constant (real part) is to be measured, and should be tested in the absence of an insulating film when the conductivity is to be measured. In case that the material is substantially conductive, the imaginary part of the relative dielectric constant can be calculated from the conductivity. This is the method used in the prior work by Chung and her students for the study of various carbon materials [13–16]. This method is also used in the present work.

The imaginary part of the relative dielectric constant (3.16–811 kHz) of GO containing sorbed water (21 wt% sorbed water) has been reported to be essentially 0 and in the range from 10 to $10^3$ under the presence and absence of an insulating film, respectively [9]. The measurement was made using an RLC meter. The essentially zero value in the presence of the insulating film is questionable, as it is not consistent with the known substantial conductivity of GO containing sorbed water [10,11]. The higher values in the absence of the insulating film are also questionable, as explained above. Therefore, clarification of the dielectric behavior of GO containing sorbed water is needed.

Another method of electrical/dielectric testing is impedance spectroscopy, which provides the variation of the real and imaginary parts of the impedance with the frequency. The resulting Nyquist plot of the imaginary part vs. real part of the impedance is then analyzed by fitting the curve in the plot with that calculated by using an equivalent electrical circuit that consists of resistors and capacitors with values that do not vary with the frequency. Through the curve fitting, the values of the resistors and capacitors are determined. From the value of the specimen resistor in the circuit, the conductivity is obtained. From the value of the specimen capacitor in the circuit, the relative dielectric constant (real part) is obtained. This method suffers from the assumption that the circuit elements have values that are independent of the frequency. In addition, the uniqueness and accuracy of the resulting resistance and capacitance values are questionable, due to the assortment of parameters (corresponding to the assortment of circuit elements) used in the curve fitting. Prior work [11] used this method.

In an electrical measurement, electrical contacts to the specimen are needed. The common configuration involves the specimen being sandwiched by two electrical contacts, as in a parallel-plate capacitor. This configuration means that the system being tested involves both the volume of the specimen and the interface between the specimen and each of the two electrical contacts. It is the volumetric information on the specimen that is being sought. Therefore, decoupling is needed between the volumetric and interfacial contributions to the measured quantity (whether capacitance or resistance). The absence of this decoupling and the consequent consideration of the measured capacitance/resistance to be entirely due to the specimen lead to the underestimation of the measured values of the relative dielectric constant (real part) and conductivity of the specimen, since the specimen and the two interfaces on its two sides are capacitors/resistors in series.

The decoupling mentioned above was not performed in the prior work that used an RLC meter for the electrical measurement [9]. In the prior work that involved impedance spectroscopy [11], the Nyquist plot obtained was fitted with an equivalent circuit model in order to extract the resistance and capacitance information of the specimen. The effectiveness of the decoupling is questionable, due to the assortment of parameters involved in the fitting. The inadequacy associated with the decoupling in prior work adds to the importance of clarifying the previously reported dielectric and conductive properties of GO containing sorbed water [9,11].

In our prior work [13], graphite oxide (GO) paper in the dried state, as obtained by heating the paper at 60 °C for 3 h immediately prior to electrical testing, was tested using an RLC meter. In contrast to the abovementioned prior work [9,11], in our prior work [13], (i) the volumetric and interfacial contributions were clearly decoupled through the testing of specimens at three different thicknesses and evaluating the slope of the curve of the inverse of the capacitance vs. the specimen thickness in case of relative dielectric constant (real part) determination, and the slope of the curve of the resistance vs. specimen thickness in case of conductivity determination, (ii) an insulating film was used in the measurement of the relative dielectric constant (real part), and (iii) an insulating film was not used in the measurement of the conductivity.

### 1.3. Objectives

This paper extends our prior work [13] on GO (referred to as $GO_{18}$, due to it water content of 18 wt%., as obtained by heating at 60 °C for 3 h immediately before testing) to the study of the effect of

sorbed water content on the electrical and dielectric properties. The methods of material preparation and electrical and dielectric testing are the same as those of our prior work [13]. The effect of the additional sorbed water is studied by comparing the electrical and dielectric properties of $GO_{18}$ [13] and $GO_{22}$ (containing 22 wt% water, i.e., the abovementioned GO tested without heating at 60 °C for 3 h immediately prior to the electrical testing).

The reduction of GO to form reduced graphite oxide (RGO) increases the conductivity and the relative dielectric constant (real part) [14]. Sorbed water addition also increases the conductivity of GO [4,7,10,11], and it has been reported to decrease the relative dielectric constant [11] and the capacitance [2]. Comparison of the effects of reduction and water addition on the electrical and dielectric behavior has not been previously reported, though it is practically important to the applications of these two materials and may shed light on the conduction and polarization mechanisms.

The objectives of this work are (i) to clarify the electrical and dielectric properties of GO containing sorbed water, particularly in view of the issues associated with prior reports [9,11], (ii) to investigate the effect of the sorbed water content on the electrical and dielectric properties of GO, and (iii) to compare the effects of reduction (to form RGO) and sorbed water content increase on the electrical and dielectric properties of GO.

## 2. Experimental methods

The approach used for achieving the decoupling mentioned in Sec. 1.2 involves (i) measuring the through-thickness resistance and capacitance of the GO paper (for determining the quantities pertaining to the non-air part of the paper), and (ii) conducting the measurement for three paper thicknesses, thereby decoupling volumetric and contact-contact interfacial quantities. The approach is the same as that of prior work in the same laboratory as this work [13–16]. The prior work concerns dried GO [13], reduced GO [14], exfoliated graphite [15–17], graphite nanoplatelet [16], carbon black [16] and activated carbon [16]. Please refer to the prior work [13] for the details of the testing set-up.

### 2.1. Materials

As in our prior work [13,14], the graphite raw material for preparing the GO is Micro 850 from Asbury Graphite Mills, Inc. (Asbury, NJ). It is natural crystalline graphite with particle size 5 μm and 99% carbon. The GO is prepared using the modified Hummers method [18]. This method involves (i) putting 22.50 g of 98% sulfuric acid ($H_2SO_4$) and 0.500 g of sodium nitrate ($NaNO_3$) powder in an open glass beaker, followed by placing the beaker in a basin of ice water for the purpose of cooling the beaker 0 °C, (ii) adding 1.000 g of graphite, followed by magnetic stirring for 30 min, while the beaker remains cooled, (iii) slowly adding 3.000 g potassium permanganate ($KMnO_4$), while the beaker remains cooled, (iv) allowing the beaker to be heated naturally (due to the exothermic reaction) to 35 °C, which is kept for 30 min while magnetic stirring takes place, with the color changing from black to dark purplish green, (v) continuing the magnetic stirring for 2 days, with the color of the dispersion changing to dark brown, (vi) slowly adding 45 ml of de-ionized water, while stirred occurs, in order to prevent violent effervescence, thereby causing the temperature to increase to 90–95 °C, which is then maintained for 15 min, (vii) adding 10.00 ml of 30% hydrogen peroxide ($H_2O_2$) and 53.00 ml of deionized water in order to reduce the residual potassium permanganate and manganese dioxide ($MnO_2$) to form soluble manganese sulfate ($MnSO_4$), with the color of the solid (GO) changing to bright yellow (characteristic of the maximally oxidized product with C:O ratio between 2.1 and 2.9 [19]), while the liquid above it is colorless, and (viii) drying the dispersion to obtain the solid (GO), which is dark brown.

The GO paper is prepared from the GO by (a) magnetically stirring the GO aqueous dispersion for 2 h, followed by allowing the dispersion to sit for 24 h for the purpose of having the GO settle down, then decanting the upper colorless water above the GO, and then adding hydrochloric acid (HCl) in the amount of 5% of the weight of the dispersion, followed by allowing the settling for 24 h and then decanting the colorless water above the GO, and then repeating all of step (a) once, (b) repeating again and again all of step (a), but using deionized water instead of hydrochloric acid until the decanted liquid has a pH close to 7, (c) sonicating thrice, with each time lasting 1.5 h, such that the color changes from bright yellow solid (before step (a)) to dark brown dispersion (after step (c)), (d) casting the dispersion into 50 × 50 mm square silicone molds with mold cavities of three different thicknesses, and then drying at room temperature for 72 h, followed by oven drying at 60 °C for 6 h.

During storage in a sealed plastic bag placed in a room at (20 ± 2)°C and (55 ± 5)% relative humidity, the prepared GO paper absorbs moisture. In this work, the $GO_{18}$ paper refers to the GO paper that was subjected to oven drying at 60 °C for 6 h immediately before testing; this is the material of our prior work [13]; it contains 18 wt% sorbed water. In contrast, $GO_{22}$ paper refers to the GO paper that was not subjected to this drying immediately prior to testing; it contains 22 wt % sorbed water.

The RGO is prepared from the abovementioned GO by chemical reduction using hydrazine hydrate. The preparation method and the electrical and dielectric properties are described in our prior report [14].

### 2.2. Sorbed water content determination

The difference in sorbed water content between $GO_{22}$ and $GO_{18}$ is obtained in this work by weighing the material before and after the drying. Comparison of the mass per unit volume of the $GO_{18}$ paper and that of the $GO_{22}$ paper shows that the additional sorbed water content (the sorbed water content beyond that in the $GO_{18}$ paper) in the $GO_{22}$ paper is (3.3 ± 0.3) wt.%, which corresponds to C/$H_2O$ mole ratio 24.6 ± 3.9, where $H_2O$ refers to the additional sorbed water.

The sorbed water contents in the $GO_{22}$ paper and $GO_{18}$ paper are separately determined by thermogravimetric analysis (TGA). Upon heating from 30 °C at a heating rate of 10 °C/min under flowing nitrogen gas at a flow rate of 19.8 mL/min, using a Perkin-Elmer Corp. 4000 TGA instrument, the first step of weight loss occurs in the temperature range from 30 to 122 °C. This weight loss is attributed to water loss, with the water being primarily interlayer water [9].

The TGA results in Fig. 1 show that the sorbed water content in the $GO_{18}$ paper is 17.9 wt% (which corresponds to C/$H_2O$ mole ratio 4.5, where $H_2O$ refers to the total sorbed water), whereas that in the $GO_{22}$ paper is 21.8 wt% (which corresponds to C/$H_2O$ mole ratio 3.7). This means that both $GO_{18}$ paper and $GO_{22}$ paper have substantial amounts of sorbed water, such that the difference in sorbed water content is 3.8 wt%, which is consistent with the value of 3.3 wt% mentioned above, based on the weighing of the $GO_{18}$ paper and $GO_{22}$ paper. The value of 3.3 wt% is more reliable than that of 3.8 wt%.

The heating above 122 °C essentially does not alter the weight difference between the two TGA curves in Fig. 1. This means that the difference between the two curves for the entire temperature range is mainly due to the difference in the amount of weight loss below 122 °C. The weight loss above 122 °C is attributed mainly to the loss of species associated with the functional groups on the surface of

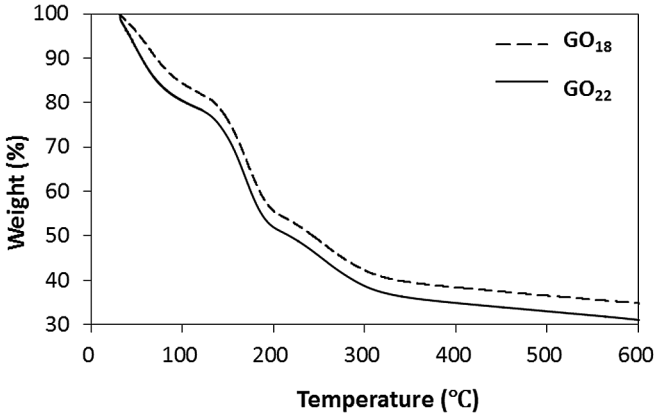


**Fig. 1.** TGA curves of $GO_{18}$ paper (dashed curve) and $GO_{22}$ paper (solid curve) during heating.

the GO [9,20]. The amounts and nature of the functional groups are apparently similar for the two materials.

### 2.3. Structural analytical method

It should be emphasized that $GO_{18}$ means GO containing 17.9 wt % sorbed water, as obtained by oven drying at 60 °C for 6 h immediately before testing. The $GO_{18}$ is the material of our prior work [13].

#### 2.3.1. vol fractions of the constituents

Under the assumption that the $GO_{22}$ paper consists of $GO_{18}$, additional sorbed water and air, the volume fraction each of these three constituents are calculated using the method described below. The calculation is based on the measured density of the $GO_{22}$ paper and that of each of the constituents, with the density of the additional sorbed water taken as 1.000 g/cm$^3$ and the density of $GO_{18}$ taken as 2.200 g/cm$^3$ [21]. The density of the $GO_{22}$ paper is (1.5706 ± 0.0046) g/cm$^3$, as obtained from the mass and volume of the $GO_{22}$ paper. The density $\rho_{wg}$ of the $GO_{22}$ paper, according to the Rule of Mixtures, is given by

$$\rho_{wg} = \rho_g v_g + \rho_w v_w, \tag{1}$$

where $\rho_g$ and $\rho_w$ are the densities of $GO_{18}$ and additional sorbed water, respectively, and $v_g$, $v_w$ and $v_a$ are the volume fractions of $GO_{18}$, additional sorbed water and air, respectively. Since there are only the three constituents,

$$v_g + v_w + v_a = 1. \tag{2}$$

Compared to the $GO_{18}$ paper, the additional sorbed water content in the $GO_{22}$ paper is (3.3 ± 0.3) wt.%. Consider 100 g of $GO_{22}$ paper. It contains 96.7 g of $GO_{18}$ and 3.3 g of additional sorbed water. Thus,

$$V_g = (96.7/2.2)\text{cm}^3 = 44.0\ \text{cm}^3, \tag{3}$$

where $V_g$ is the volume of $GO_{18}$, and

$$V_w = 3.3/1.0 = 3.3\ \text{cm}^3, \tag{4}$$

where $V_w$ is the volume of the additional sorbed water.

Hence,

$$V_w/V_g = v_w/v_g = 3.3/44.0 \tag{5}$$

By using the three simultaneous equations in Eqs. (1), (2) and (5), the three unknowns, which are the volume fractions of $GO_{18}$, additional sorbed water and air, are obtained. Thus, the volume fractions of the three constituents of the $GO_{22}$ paper are found to be (69.03 ± 0.25) vol% $GO_{18}$, (5.19 ± 0.51) vol% additional sorbed water, and (25.78 ± 0.38) vol% air. In other words, the non-air part of the $GO_{22}$ paper amounts to (74.22 ± 0.38) vol%.

#### 2.3.2. Relative dielectric constant (real part) calculation based on the volume fractions of the constituents

Under the assumption that the three constituents of the $GO_{22}$ paper are capacitors in parallel (Fig. 2(a)), the relative dielectric constant $\kappa_{wg}$ of the $GO_{22}$ paper, according to the Rule of Mixtures, is given by

$$\kappa_{wg} = \kappa_g v_g + \kappa_w v_w + \kappa_a v_a, \tag{6}$$

where the relative dielectric constant $\kappa_w$ of additional sorbed water is taken to be 80 [16] and the relative dielectric constant $\kappa_a$ of air is 1.000. By using Eq. (6) and the relative dielectric constant of $GO_{18}$ determined in our prior work [13], the relative dielectric constant $\kappa_{wg}$ of the $GO_{22}$ paper is calculated. This is the calculated value based on the assumption of capacitors in parallel.

Under the assumption of capacitors in series (Fig. 2(b)), the relative dielectric constant of the $GO_{22}$ paper, according to the Rule of Mixtures, is given by

$$1/\kappa_{wg} = v_g/\kappa_g + v_w/\kappa_w + v_a/\kappa_a. \tag{7}$$

By using Eq. (7), the relative dielectric constant of the $GO_{22}$ paper is calculated. This is the value based on the assumption of capacitors in series.

### 2.4. Electrical characterization methods

#### 2.4.1. Experimental set-up

Unless noted otherwise, the reported results are for the through-thickness direction. For both through-thickness and in-plane electrical measurements, specimens at three thicknesses are tested. The three thicknesses of $GO_{22}$ paper are 0.114 ± 0.003 mm, 0.248 ± 0.003 mm, and 0.364 ± 0.003 mm; they correspond to specimen masses of 70.72 ± 0.01 mg, 156.29 ± 0.01 mg, and 228.89 ± 0.01 mg, respectively.

Each $GO_{22}$ paper specimen for the through-thickness dielectric/conductivity testing is a square with dimension 20.00 ± 0.10 mm at each edge of the square, as obtained by cutting and removing the four edge regions from the molded 50 × 50 mm square specimen.

Each specimen for in-plane electrical conductivity testing is a rectangular strip of width 4.840 ± 0.003 mm, and length exceeding 30.000 mm. The four-probe method is used, with the two inner voltage contacts being 19.200 ± 0.003 mm apart and two outer current contacts being 28.000 ± 0.003 mm apart and symmetrically positioned relative to the two inner contacts. All four contacts are made with silver paint in conjunction with copper wires.

Fig. 2 shows the equivalent electrical circuit used in this work for modeling the through-thickness conduction and dielectric behavior of the $GO_{22}$ paper. In this circuit, $GO_{18}$, air and additional sorbed water are electrically in parallel and this parallel combination is in series with both electrical contacts, which are in contact with the two opposite surfaces of the $GO_{22}$ paper, thereby sandwiching the paper. All the quantities shown in the model are decoupled and determined using the method of prior work [13].

The through-thickness relative dielectric constant (which describes the volumetric dielectric behavior of the paper), the specific interfacial capacitance (which is the capacitance per unit area of the

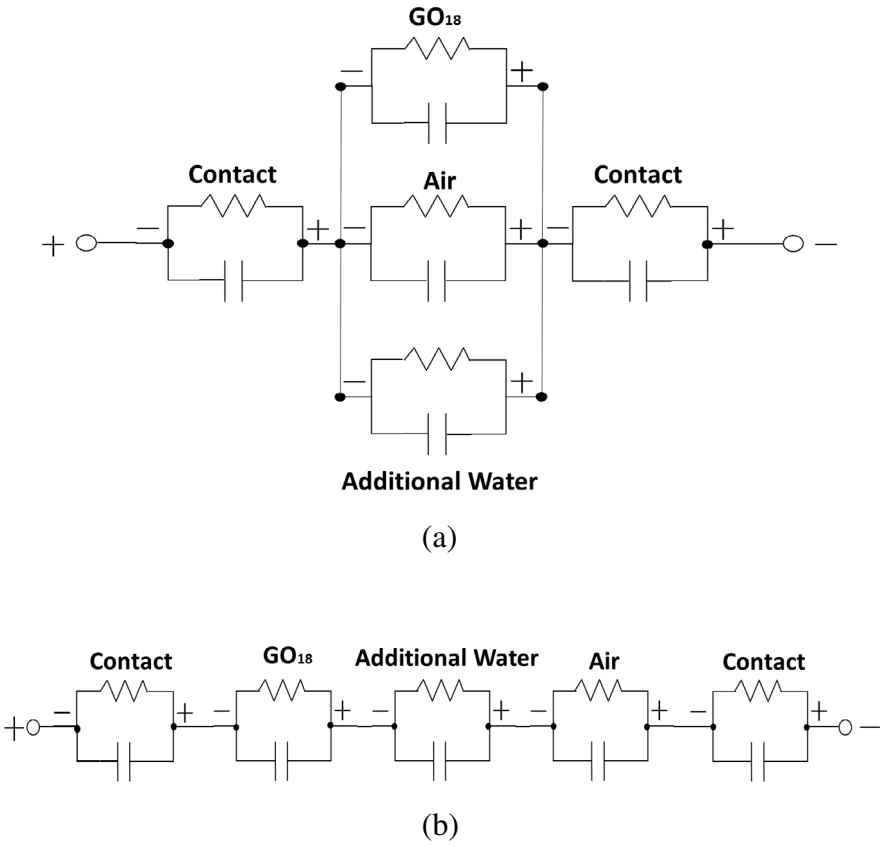


**Fig. 2.** Equivalent electrical circuit models for the through-thickness electrical behavior of the $GO_{22}$ paper. The contact refers to the interface between the paper and an electrical contact. (a) Parallel model. (b) Series model.

interface between the paper and either electrical contact), the through-thickness electrical resistivity (which describes the geometry-independent through-thickness volumetric conduction behavior of the paper) and the interfacial electrical resistivity (which is the geometry-independent areal resistivity of the interface between the paper and either electrical contact) are measured in this work, using a precision RLC meter (Quadtech 7600), with the frequency ranging from 50 Hz to 2 MHz. The capacitance and resistance for the parallel RC circuit configuration are separately obtained from the meter, such that the capacitance is measured with an electrically insulating film (thickness 75 μm) between the paper and each electrical contact, and the resistance is measured without this insulating film [13]. The use of the electrically insulating film in case of capacitance measurement is for the purpose of minimizing the through-thickness current, as needed for the RLC meter to function properly, thereby determining essentially the real part of the relative dielectric constant. The AC voltage is adjusted so that the electric field is fixed at 22.6 V/cm while the thickness varies, so the voltage is 0.50, 0.90 and 1.26 V for the three thicknesses.

In order to decouple the volumetric and interfacial contributions to the capacitance, specimens of three different thicknesses are tested. The electric field is applied between two copper foils (thickness 62 μm), which are the electrical contacts. The pressure provided by a copper foil and a steel weight (above the foil) on the paper during testing is 4.3 kPa (0.63 psi).

The decoupling of the contribution of $GO_{18}$, additional sorbed water and air is performed by using the Rule of Mixtures, with three constituents modeled as being electrically in parallel (Fig. 2(a)). The series model (Fig. 2(b)) is much less effective than the parallel model for fitting with the experimental results presented in this paper. The superiority of the parallel model is consistent with the fact that the carbon layers in GO are not flat and the contacts between the adjacent layers allow conduction and polarization in the direction perpendicular to the layers.

### 2.4.2. Capacitance analytical method

The volumetric capacitance of the GO paper ($C_v$) and the capacitance of the interface between the paper and an electrical contact ($C_i$) are in series, so the measured capacitance $C$ is given by

$$1/C = 2/C_i + 1/C_v. \tag{8}$$

The factor of 2 in Eq. (8) is due to the presence of two interfaces on the two sides of the paper. Due to Eq. (8), $C_i$ is less influential when it is large. The $C_v$ is given by

$$C_v = \varepsilon_0 \kappa A/l, \tag{9}$$

where $\varepsilon_0$ is the permittivity of free space ($8.85 \times 10^{-12}$ F/m), $\kappa$ is the through-thickness relative dielectric constant of the paper, $A$ is the paper area ($20.0 \times 20.0$ mm$^2$), and $l$ is the paper thickness. The $\kappa$ is the same as the real part (commonly abbreviated $\kappa'$) of the relative dielectric constant.

Due to Eqs. (8) and (9), the plot of $1/C$ against $l$ is a straight line with the intercept of $2/C_i$ at the $1/C$ axis at $l = 0$, and the value of $\kappa$ is obtained from the slope, which is equal to $1/(\varepsilon_0 \kappa A)$. Using the model of capacitors in parallel, the interfacial capacitance $C_i$ of the interface between the specimen and the electrical contact is given by

$$C_i = C_{ig} + C_{iw} + C_{ia} \tag{10}$$

where $C_{ig}$ is the interfacial capacitance associated with $GO_{18}$, $C_{iw}$ is the interfacial capacitance associated with the additional sorbed water and $C_{ia}$ is the interfacial capacitance associated with air part. The $C_{ia}$ is neglected, due to the thickness of the air gap resulting in a low capacitance. The air gap is discontinuous in the plane of the interface, but its thickness is expected to be of the order of the undulation in the carbon layers. The undulation is considerable, as suggested by the breadth of the XRD peak (Fig. 2 of this paper and Fig. 2 of Ref. [13]), the substantial intensity of the disordered (D) Raman peak (Fig. 3), and microscopy images (not included). Thus, Eq. (10) is approximated as

$$C_i = C_{ig} + C_{iw} = C_{iwg}, \tag{11}$$

where $C_{iwg}$ is the capacitance associated with the non-air part. The specific interfacial capacitance $C_c$ of $GO_{22}$ is given by

$$C_c = C_i / [(1 - a_a)A], \tag{12}$$

where $a_a$ is the area fraction (approximately equal to the volume fraction) of the air part and $A$ is the area of the overall electrical contact.

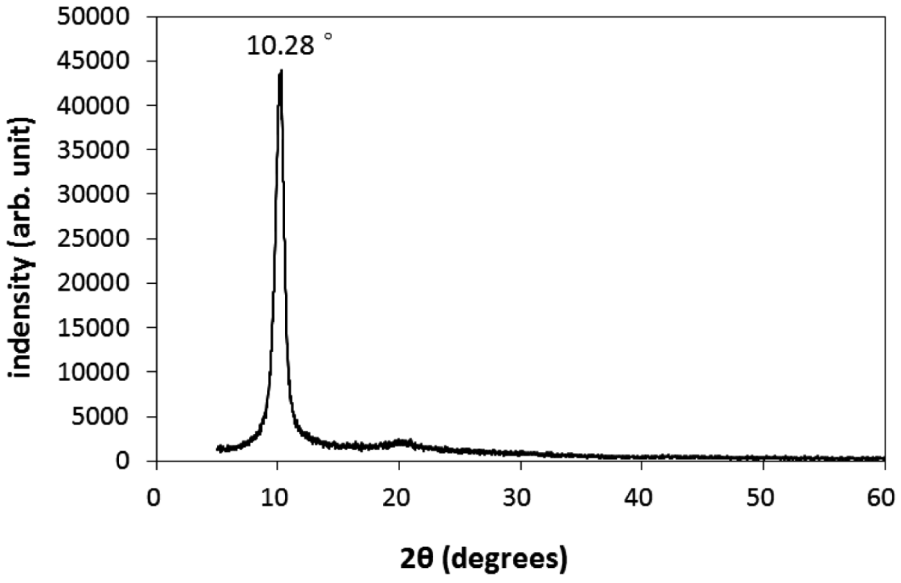


(a)

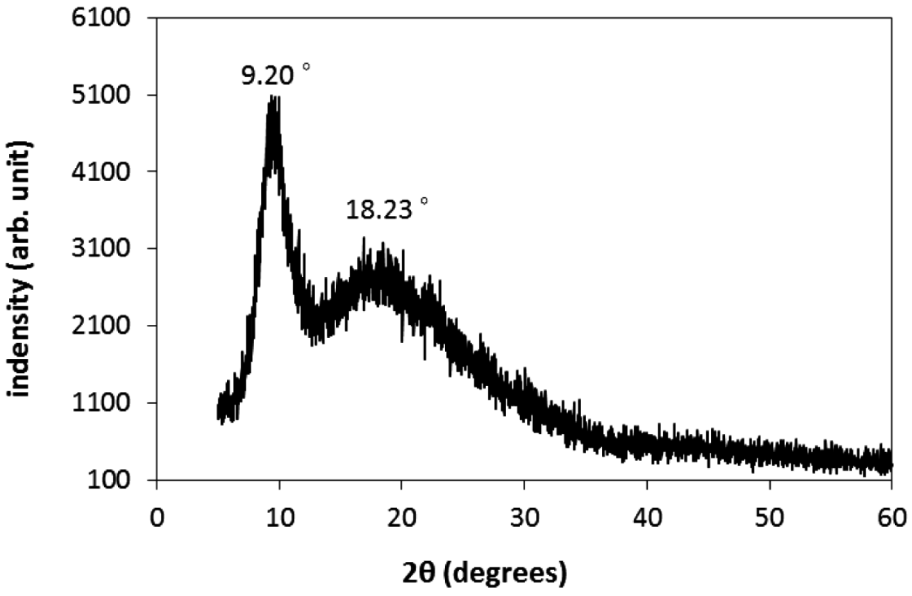


(b)

**Fig. 3.** X-ray diffraction (XRD) pattern of (a) $GO_{18}$ paper, and (b) $GO_{22}$ paper.

The non-air part (i.e., entirety minus air) of the $GO_{18}$ paper refers to $GO_{18}$, with the air excluded. Also based on the parallel model, with the contribution of air to the relative dielectric constant neglected, the relative dielectric constant $\kappa_g$ of the non-air part of the $GO_{18}$ paper is given by

$$\kappa_g = \kappa_{dp}/(1 - v_a), \tag{13}$$

where $\kappa_{dp}$ is the relative dielectric constant of the $GO_{18}$ paper.

Considering that the $GO_{22}$ paper is electrically equivalent to $GO_{18}$, additional sorbed water and air in parallel in the through-thickness direction, the capacitance $C_{wp}$ of the $GO_{22}$ paper is given by

$$C_{wp} = C_g + C_w + C_a, \tag{14}$$

where $C_g$, $C_w$ and $C_a$ are the capacitances of $GO_{18}$, additional sorbed water and air, respectively. The relative dielectric constant $\kappa_{wp}$ of the $GO_{22}$ paper is given by Eq. (6). Using the measured value of the relative dielectric constant of the $GO_{22}$ paper, the relative dielectric constant of $GO_{18}$ obtained in our prior work [13], the volume fractions of the three constituents, and Eq. (6), the effective relative dielectric constant $\kappa_w$ of the additional sorbed water in the $GO_{22}$ paper is calculated.

The non-air part (i.e., the entirety minus the air part) of the $GO_{22}$ paper refers to the combination of $GO_{18}$ and additional sorbed water, with the air excluded. Also based on Eq. (6) and the parallel model, the relative dielectric constant $\kappa_{wg}$ of the non-air part of the $GO_{22}$ paper is given by

$$\kappa_{wg} = \left(\kappa_g v_g + \kappa_w v_w\right)/(1 - v_a) = \left(\kappa_{wp} - \kappa_a v_a\right)/(1 - v_a). \tag{15}$$

The relative dielectric constant reported here includes the value $\kappa_{wp}$ for the overall $GO_{22}$ paper and the value $\kappa_{wg}$ for the non-air part of the $GO_{22}$ paper.

### 2.4.3. Resistance analytical method

The measured resistance $R$ between the two copper contacts that sandwich the GO paper includes the through-thickness volume resistance $R_v$ of the paper and the resistance $R_i$ of each of the two interfaces between the paper and a copper contact, i.e.,

$$R = R_v + 2R_i. \tag{16}$$

By measuring $R$ at three paper thicknesses, the curve of $R$ versus thickness is obtained. The intercept of this curve with the $R$ axis at zero thickness equals $2R_i$, whereas the slope of this curve equals $R_v/l$, where $R_v$ is the paper resistance for the paper thickness of $l$. The through-thickness GO paper resistivity is obtained by multiplying $R_v/l$ by the specimen area $A$. The paper conductivity is the inverse of the paper resistivity.

The non-air part (i.e., entirety minus air) of the $GO_{18}$ paper refers to $GO_{18}$ with the air excluded. Also based on the parallel model, the conductivity $\sigma_g$ of the non-air part of the $GO_{18}$ paper is given by

$$\sigma_g = \sigma_{dp}/(1-v_a), \tag{17}$$

where $\sigma_{dp}$ is the conductivity of the $GO_{18}$ paper. The conductivity reported in our prior work [13] includes the value $\sigma_{dp}$ for the overall $GO_{18}$ paper and that $\sigma_g$ for the non-air part of the $GO_{18}$ paper.

Considering that the $GO_{22}$ paper is electrically equivalent to $GO_{18}$, additional sorbed water and air in parallel in the through-thickness direction, the conductivity $\sigma_{wp}$ of the $GO_{22}$ paper is given by

$$\sigma_{wp} = \sigma_g v_g + \sigma_w v_w. \tag{18}$$

where $\sigma_g$ and $\sigma_w$ are the conductivities of $GO_{18}$ and the additional sorbed water, respectively. Using the measured value of the conductivity $\sigma_{wp}$ of the $GO_{22}$ paper, the conductivity $\sigma_g$ of the $GO_{18}$ obtained in our prior work [13] and Eq. (18), the effective conductivity $\sigma_w$ of the additional sorbed water in the $GO_{22}$ paper is calculated.

The conductivity $\sigma_{wg}$ of the non-air part of $GO_{22}$ paper is given by

$$\sigma_{wg} = \sigma_{wp}/(1-v_a). \tag{19}$$

The conductivity reported here includes the value $\sigma_{wp}$ for the overall $GO_{22}$ paper and the value $\sigma_{wg}$ for the non-air part of the $GO_{22}$ paper.

Based on the parallel model, the interfacial resistance $R_i$ (the resistance of the interface between the specimen and the electrical contact) is given by

$$1/R_i = 1/R_{ig} + 1/R_{iw} + 1/R_{ia}, \tag{20}$$

where $R_{ig}$ is that interfacial resistance associated with the $GO_{18}$, $R_{iw}$ is that associated with the additional sorbed water and $R_{ia}$ is that associated with the air part. Since $R_{ia}$ is infinity, the last term of Eq. (20) is negligible and Eq. (20) becomes

$$1/R_i = 1/R_{ig} + 1/R_{iw} = 1/R_{iwg}, \tag{21}$$

where $R_{iwg}$ is the resistance of the non-air part of the interface. The interfacial resistivity $\rho_{iwg}$ of the non-air part of the interface between $GO_{22}$ and the electrical contact is thus given by

$$\rho_{iwg} = R_{iwg}(1 - a_a)A. \tag{22}$$

Combination of Eqs. (21) and (22) gives

$$\rho_{iwg} = R_i(1 - a_a)A. \tag{23}$$

For the sake of simplicity, $\rho_{iwg}$ is referred to as $\rho_i$.

### 2.4.4. Dielectric loss analytical method

For a conductive material, the conduction loss dominates the energy loss, so the imaginary part $-\kappa''$ (where $\kappa''$ is negative) of the relative dielectric constant is related to the conductivity $\sigma$ by the equation

$$-\kappa'' = \sigma/(2\pi v \varepsilon_0), \tag{24}$$

where $v$ is the AC frequency. In this work, $\sigma$ in Eq. (24) is the conductivity of the non-air part of the $GO_{22}$ paper, so $-\kappa''$ obtained from Eq. (24) is the value for the non-air part of the $GO_{22}$ paper. Eq. (24) is valid, at least approximately, due to the substantial conductivity of the $GO_{22}$ paper and the consequent dominance of the conduction contribution to the imaginary part of the relative permittivity. For the $GO_{18}$ paper, as shown in our prior work [13], the conductivity is much lower than the $GO_{22}$ paper of this work, so the validity of Eq. (24) is questionable for the $GO_{18}$ paper.

The dielectric loss (tan $\delta$) is obtained by using the equation

$$\tan\delta = -\kappa''/\kappa' = \sigma/(2\pi v \varepsilon_0 \kappa'), \tag{25}$$

where $\kappa'$ is the real part of the relative dielectric constant. In this work, $\sigma$ in Eq. (25) is the conductivity of the non-air part of the $GO_{22}$ paper, so tan $\delta$ obtained from Eq. (25) is the value for the non-air part of the $GO_{22}$ paper.

## 3. Results and discussion

### 3.1. Structure of the GO paper

The GO paper is dark brown in color. With the true density of GO taken to be 2.200 g/cm$^3$ [21], the non-air content in the GO paper is (69.03 ± 0.25) vol% [13] and (74.22 ± 0.38) vol% for $GO_{18}$ [13] and $GO_{22}$ respectively. Please refer to Sec. 2.3.1 for the calculation of the non-air content of the $GO_{22}$ paper.

The elemental composition of the $GO_{18}$ paper [13], as determined by energy dispersive x-ray spectroscopy in conjunction with scanning electron microscopy, is shown in Table 1. The carbon/oxygen atomic ratio is 1.95 ± 0.23. This ratio, and the atomic concentrations of C and O, are all close to those of prior work on GO [22]. The minor amount of sulfur (2.43 ± 0.40 at.%) is attributed to the sulfuric acid used in the GO preparation.

For the $GO_{18}$ paper, comparison of the C/$H_2O$ mole ratio (with the water referring to the total sorbed water) of 4.5 (Sec. 2.2) and the C/O atomic ratio of 2.0 indicates that the O/$H_2O$ mole ratio is 2.3. This implies that all 44% of the oxygen atoms in $GO_{18}$ correspond to water molecules.

For the $GO_{22}$ paper, the C/$H_2O$ mole ratio (with the water referring to the total sorbed water) is 3.7 (Sec. 2.2). By considering the C/$H_2O$ mole ratio of 4.5 for the $GO_{18}$ paper (Sec. 2.2), which has a C/O ratio of 2.0, one obtains by proportion that all 53% [i.e., 44% (4.5/3.7)] of the oxygen atoms in $GO_{22}$ correspond to water molecules. It is reasonable to assume that the additional sorbed water (which is minor in quantity) does not affect the C/O ratio of the graphite oxide, in which the oxygen atoms are strongly bonded to the carbon atoms.

Comparison of the C/$H_2O$ mole ratio of 25 (for the additional sorbed water) (Sec. 2.2) and the C/O atomic ratio of 2.0 indicates that the O/$H_2O$ mole ratio is 13 for the additional sorbed water. This implies that all 8% of the oxygen atoms in $GO_{22}$ correspond to additional sorbed water molecules. Thus, all 52% (44% + 8%) of the oxygen atoms in $GO_{22}$ correspond to water molecules (among those in the total water). Hence, the values for the fraction of oxygen atoms in $GO_{22}$ corresponding to a water molecule (any of the water molecules in the total water), as obtained by the method of this paragraph and the method of the last paragraph, are close.

X-ray diffraction (XRD) of the $GO_{18}$ paper (Fig. 3(a)) shows the main peak at $2\theta = 10.28°$. This corresponds to an interlayer spacing of 8.60 Å. The amount of sorbed water affects the interlayer spacing of GO [8], so there is variability in the interlayer spacing among different published works.

In addition, Fig. 3(a) shows a weak broad peak at 20.5° corresponding to an interlayer spacing of 4.33 Å for the $GO_{18}$ paper. The weak peak has been previously reported in GO with C/O ratio 2.47 and interpreted as being due to the incomplete intercalation of a minor part of the material [23]. However, the absence of a graphite 002 peak in Fig. 3(a) indicates the absence of residual graphite.

Fig. 3(b) shows that the $GO_{22}$ paper exhibits the main XRD peak at $2\theta = 9.20°$, which corresponds to an interlayer spacing of 9.61 Å. This spacing is higher than the value for the $GO_{18}$ paper (Fig. 3(a)). That the interlayer spacing is higher for the $GO_{22}$ paper is as expected. The $GO_{22}$ paper also exhibits a broad XRD peak at $2\theta = 18.23°$, which corresponds to an interlayer spacing of 4.86 Å. Such a broad peak at this position has been previously reported for GO that contains a minor amount of residual graphite, which is shown by a weak peak at $2\theta = 26°$ [20]. A weak peak at $2\theta = 18°$ has also been observed in GO and interpreted as being due to incomplete intercalation [23]. However, Fig. 3(b) does not show any residual graphite peak. Nevertheless, the additional sorbed water accentuates and broadens this peak at 18°. Indeed, this peak has also been interpreted as being due to water domains [24].

**Table 1**
The elemental composition of $GO_{18}$, as determined by x-ray energy-dispersive spectroscopy [13].

| Element | Wt.% | At.% | C/O atomic ratio |
|---|---|---|---|
| C | 56.09 ± 1.98 | 64.52 ± 2.14 | 1.95 ± 0.23 |
| O | 38.26 ± 2.81 | 33.04 ± 2.49 | |
| S | 5.65 ± 0.92 | 2.43 ± 0.40 | |

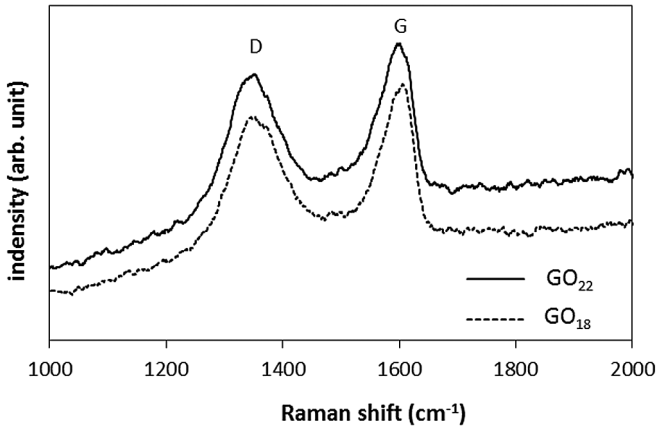


**Fig. 4.** Raman spectra of $GO_{18}$ paper (dashed curve) and $GO_{22}$ paper (solid curve).

Fig. 4 shows that the Raman spectrum is essentially identical between $GO_{18}$ paper and $GO_{22}$ paper. The ratio of the D peak to the G peak is the same at 1.00 for these two cases. This means that the additional sorbed water essentially does not affect the lattice vibrations or the degree of order of the carbon material.

As indicated by FTIR (Fig. 5), the $GO_{18}$ paper and $GO_{22}$ paper are comparable in the amounts and types of functional groups. For example, they are comparable in the amount of −CO groups. However, $GO_{22}$ has a greater amount of −OH groups than $GO_{18}$. The similarity in FTIR results is consistent with that in the Raman results.

### 3.2. Through-thickness relative dielectric constant (real part)

Fig. 6 shows that the plots of 1/*C* vs. specimen thickness is linear, as expected. The slope of the plot relates to the relative dielectric constant (real part).

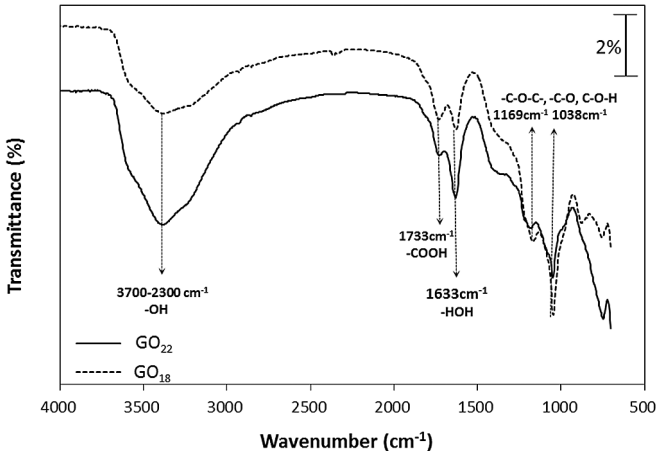


**Fig. 5.** FTIR spectrum of $GO_{18}$ paper (dashed curve) and $GO_{22}$ paper (solid curve).

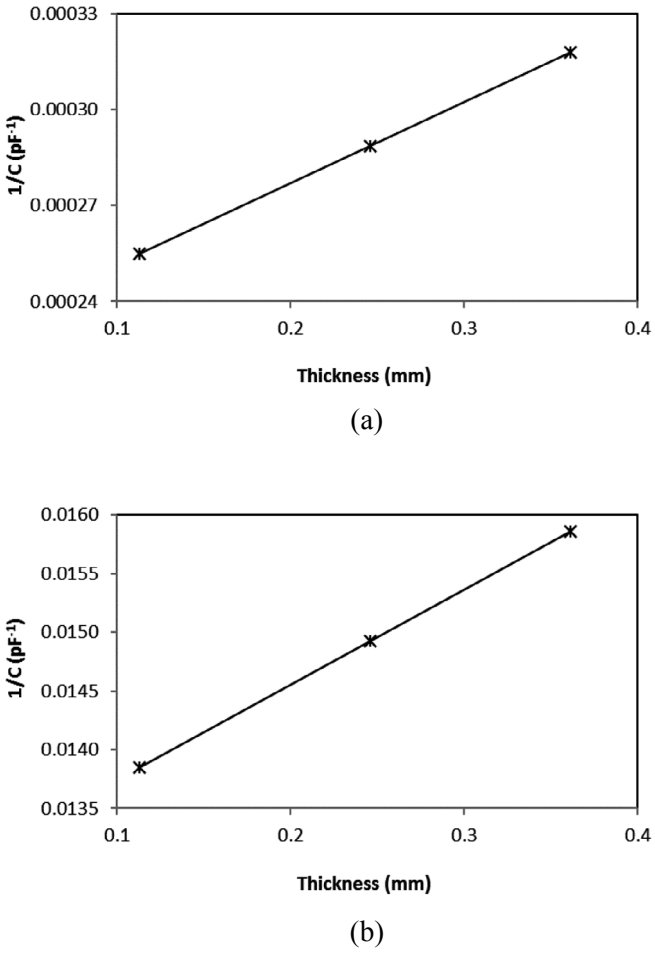


**Fig. 6.** Plot of $1/C$ (where $C$ is the measured capacitance) vs. the specimen thickness for the $GO_{22}$ paper of three different thicknesses for the determination of the through-thickness relative dielectric constant. The error bars are included, though they are too short to be clearly shown. (a) 50 Hz. (b) 2 MHz.

Fig. 7(a) and (b) show the relative dielectric constant (real part) vs. the frequency for the overall $GO_{22}$ paper (with the air included) and the non-air part of the GO paper, respectively. Comparison of Fig. 7(a) and (b) shows that, at any frequency, the relative dielectric constant (real part) of the overall $GO_{22}$ paper is lower than that of the non-air part of the paper. This is expected, due to the air in the overall $GO_{22}$ paper.

At low frequencies (<200 Hz), the relative dielectric constant (real part) is higher for $GO_{22}$ than $GO_{18}$, due to the polarizability of the additional sorbed water in $GO_{22}$ (Fig. 7(b)). However, at high frequencies (>200 Hz), it is lower for $GO_{22}$ than $GO_{18}$, suggesting that the additional sorbed water in $GO_{22}$ contributes to inhibiting the excursion of the electrons in the GO during polarization at frequencies at which the water molecules are not able to contribute to the polarization.

The decrease of the relative dielectric constant (real part) by the additional sorbed water at >200 Hz is apparently consistent with the trend of this quantity (assumed to be independent of the frequency in the analysis) in prior work [11]. It is also apparently consistent with the previously reported decrease of the capacitance (at an unspecified frequency) with increasing humidity [2]. The dielectric constant was not even reported in Ref. [2]. Therefore, comparison of the results of this work with those of prior work [2,11] cannot be effectively conducted.

The value of the relative dielectric constant (real part) for the $GO_{22}$ paper decreases sharply with increasing frequency, due to the dipole friction associated with the water molecules. For the $GO_{18}$ paper, the relative dielectric constant does not decrease with increasing frequency as precipitously.

The difference in dielectric constant between $GO_{22}$ and $GO_{18}$ decreases with increasing frequency above 1 kHz, so that, above 0.1 MHz, the values are quite close (Fig. 7(b)). That the values for $GO_{22}$ and $GO_{18}$ become close at high frequencies is attributed to the small distance of excursion of the electrons at high frequencies and the consequent reduced inhibiting influence of the additional sorbed water to the excursion.

Based on impedance spectroscopy, it has been reported that increase in the relative humidity from 40% to 100% decreases the relative dielectric constant (real part, frequency independent in the analysis) from 100 to 8 [11]. The values of the relative dielectric constant (real part, obtained in this work) are much higher than those based on impedance spectroscopy [11].

Reduced graphite oxide (RGO) has been previously studied using the same method as this work [14]. The relative dielectric constant (real part) is lower for $GO_{22}$ that RGO at high frequencies (>500 Hz), but is higher for $GO_{22}$ than RGO at low frequencies (<500 Hz) (Fig. 7(a) and (b) and Table 4). This reflects that the sorbed water is able to contribute to the relative dielectric constant (real part) only at low frequencies.

Fig. 7(c) shows the specific interfacial capacitance $C_c$ (of the non-air part of the $GO_{18}$ or $GO_{22}$ GO paper) of the interface with the electrical contact. The value is lower for $GO_{22}$ than $GO_{18}$, except for the lowest frequency of 50 Hz. This means that the presence of additional sorbed water decreases the interfacial capacitance, probably because it thickens this interface. A higher value is desirable, as it would make the interface less influential to the overall measured capacitance. The specific interfacial capacitance decreases with increasing frequency more precipitously for $GO_{22}$ than $GO_{18}$, because of the dipole friction associated with the water molecules in the $GO_{22}$ case.

At any of the frequencies studied, the specific interfacial capacitance is higher for $GO_{18}$ or $GO_{22}$ than RGO [14], such that the difference is more significant at low frequencies than high frequencies (Fig. 7(c) and (d) and Table 4). Since the effect of the sorbed water decreases with increasing frequency, this suggests that the sorbed water in $GO_{18}$ or $GO_{22}$ is mainly responsible for the high specific interfacial capacitance of $GO_{18}$ or $GO_{22}$. This further suggests that water resides at this interface and its presence there increases the specific interfacial capacitance.

As shown in Table 2, the measured and calculated (parallel model, Eq. (6), Fig. 2(a)) values of the relative dielectric constant (real part) of $GO_{22}$ (with the air included) are not far apart at 100 and 200 Hz, but are quite far apart at frequencies above and below these frequencies. The calculated values based on the series model (Eq. (7), Fig. 2(b)) are all very low compared to the corresponding measured values. This means that the parallel model is much superior to the series model, even though the preferred orientation of the carbon layers in the plane of the paper suggests the greater suitability of the series model. This suggests a degree of electrical connectivity in the through-thickness direction, as expected from the bent morphology of the carbon layers [25].

The superiority of the parallel model to the series model has been previously reported for the thermal conductivity of continuous glass fiber epoxy-matrix composite laminates in the through-thickness direction [26]. Although the glass fibers are in the plane of the laminate, the bending of the fibers causes touching of the fibers in the through-thickness direction. As a result of the

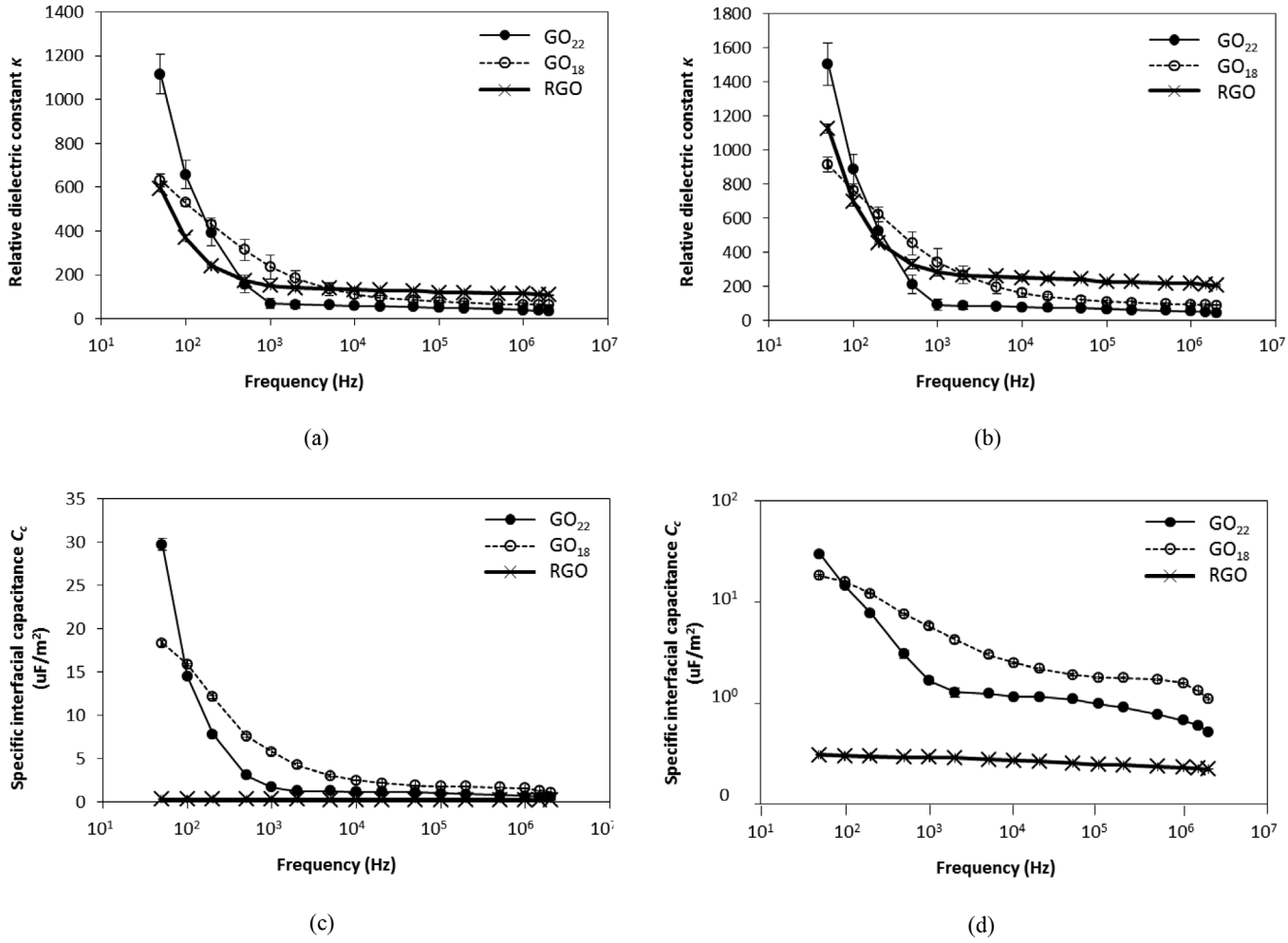


**Fig. 7.** Plot of the through-thickness relative dielectric constant $\kappa$ of the $GO_{18}/GO_{22}$/RGO paper vs. the frequency. (a) The overall $GO_{18}/GO_{22}$/RGO papers (with the air included). (b) The non-air part of the $GO_{18}/GO_{22}$/RGO papers. (c) Plots of the through-thickness specific interfacial capacitance $C_c$ for the non-air part of the $GO_{18}/GO_{22}$/RGO paper vs. the frequency. (d) Same plots as (c) except that the vertical scale is logarithmic rather than being linear in order to show the RGO data more clearly. The results for the $GO_{18}$ and RGO papers are from our prior work [13,14].

touching, the parallel model with the parallel conduction paths in the through-thickness direction is effective for explaining the measured through-thickness thermal conductivity, while the series model is less effective.

The overestimation of the relative dielectric constant (real part) of $GO_{22}$ (with the air included) at high frequencies $\geq$200 Hz, as shown by the high calculated value (parallel model) compared to the corresponding measured value (Table 2), is attributed to the fact that the relative dielectric constant of water at high frequencies is actually less that the assumed value of 80. The underestimation at low frequencies $\leq$100 Hz (Table 2) is probably due effective value is positive and extraordinarily high (much higher than the value of 80 for ordinary water) at frequencies $\leq$200 Hz, such that the value increases with decreasing frequency. This suggests that the interaction between the additional sorbed water molecules and the functional groups of the GO [4] intensifies as the frequency decreases. The effective value is negative at frequencies $\geq$500 Hz, such that the magnitude increases with increasing frequency. This suggests another type of interaction (presently unclear) that occurs at high frequencies. However, the inadequacy of the Rule of Mixtures

**Table 2**
The measured and calculated values of the through-thickness relative dielectric constant (real part) of $GO_{22}$ (with the air included) and the measured values of the through-thickness relative dielectric constant of $GO_{18}$ (with the air excluded). The parallel and series models are illustrated in Fig. 2(a) and (b) respectively. The calculation assumes that the relative dielectric constant of water is 80 at all frequencies.

| Frequency (Hz) | $GO_{22}$ | | | $GO_{18}$ [13] | Additional sorbed water |
|---|---|---|---|---|---|
| | Measured | Calculated (parallel model) | Calculated (series model) | Measured | Effective value[a] |
| 1000 | 70 ± 23 | 241 ± 56 | 3.84 ± 0.90 | 343 ± 81 | −2740 |
| 500 | 158 ± 39 | 319 ± 48 | 3.85 ± 0.58 | 455 ± 68 | −1770 |
| 200 | 392 ± 58 | 435 ± 30 | 3.85 ± 0.26 | 624 ± 43 | 2510 |
| 100 | 658 ± 64 | 533 ± 15 | 3.86 ± 0.11 | 766 ± 22 | 8050 |
| 50 | 1117 ± 92 | 636 ± 29 | 3.86 ± 0.17 | 915 ± 41 | 18900 |

[a] Calculated value, as needed to make the $GO_{22}$ calculated value based on the parallel model equal to the measured value.

may have contributed to causing these extraordinary values of the effective relative dielectric constant.

### 3.3. Through-thickness electrical conductivity

Fig. 8 shows that the plots of *R* vs. specimen thickness is linear, as expected. The slope of the plot relates to the inverse of the electrical conductivity.

Fig. 9(a) shows that the conductivity at any frequency is higher for the non-air part of the $GO_{22}$ paper than that of the $GO_{18}$ paper. This is as expected, due to the conductivity of the additional sorbed water in the $GO_{22}$ paper. Fig. 9(a) also shows that the conductivity increases with increasing frequency. This is consistent with the previous report of the impedance of GO decreasing with increasing frequency [1]. This trend of the conductivity is probably because of the decreasing excursion of the charge carriers in a cycle when the frequency increases and the consequent reduced chance for the carriers to encounter defects. The increase of the conductivity with increasing frequency is more precipitous for the $GO_{18}$ paper than the $GO_{22}$ paper, probably because the presence in $GO_{22}$ of additional sorbed water, which is conductive, reduces the effect of the defects.

At any frequency in the range studied (50 Hz–2 MHz), the through-thickness conductivity of $GO_{22}$ (0.35–1.09 S/m) is lower than that of RGO (1.17–1.61 S/m) [14] (Fig. 9(a) and Table 4). This means that the ionic conductivity of the sorbed water is not enough for $GO_{22}$ to be as conductive as RGO.

Table 3 shows the effective conductivity of the additional sorbed water, as calculated by using Eq. (16). It is higher than the conductivity of ordinary water or an aqueous solution of 15 vol% hydrochloric acid [16] by numerous orders of magnitude. This

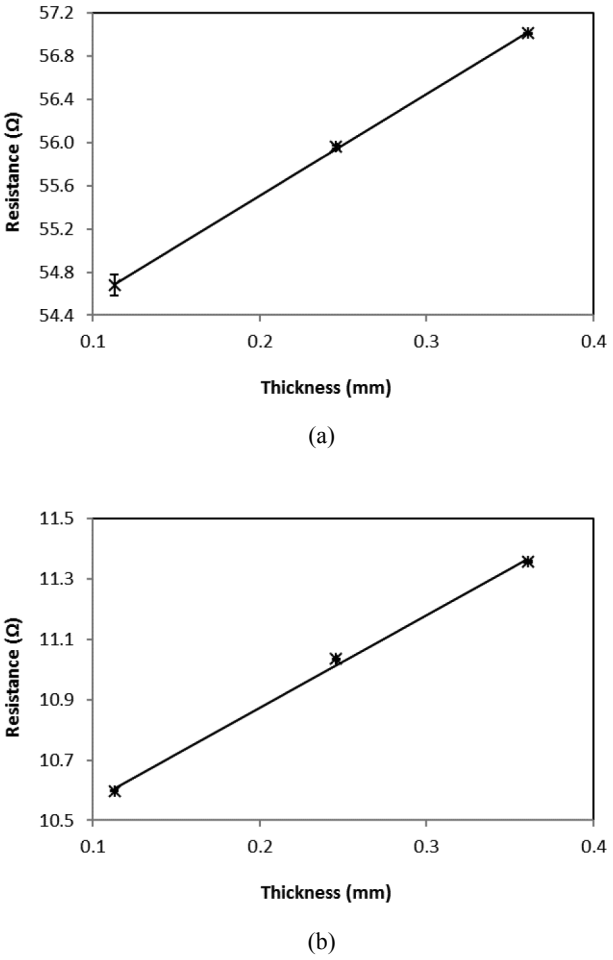


**Fig. 8.** Plot of the measured through-thickness resistance *R* vs. the specimen thickness for the $GO_{22}$ paper of three different thicknesses for the determination of the through-thickness electrical resistivity. The error bars are shown, though they are too short to be shown clearly. (a) 50 Hz. (b) 2 MHz.

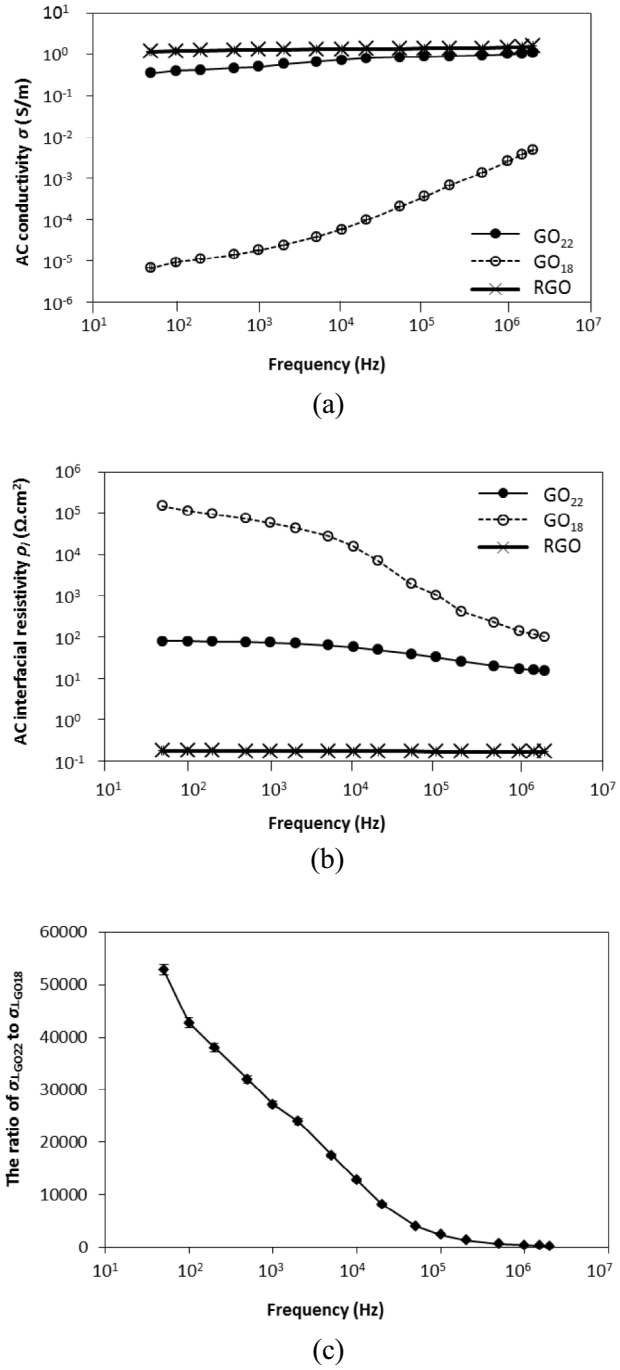


**Fig. 9.** (a) Plots of the AC conductivity vs the frequency for the non-air part of the $GO_{18}/GO_{22}$/RGO paper. (b) Plots of the AC interfacial resistivity vs. frequency for the non-air part of the $GO_{18}/GO_{22}$ paper. (c) The ratio of the through-thickness conductivity of the non-air part of the $GO_{22}$ paper $\sigma_{\perp GO22}$ to that of the $GO_{18}$ paper $\sigma_{\perp GO18}$ vs. the frequency. The results for the $GO_{18}$ paper are from our prior work [13].

**Table 3**
Conductivity of the $GO_{22}$ paper (this work), $GO_{18}$ [13] and additional sorbed water (this work). The conductivity of the additional sorbed water is the effective conductivity calculated by using Eq. (16).

| Frequency (Hz) | $GO_{22}$ paper (with air included) (S/m) | $GO_{18}$ ($10^{-6}$ S/m) [13] | Water (S/m) |
|---|---|---|---|
| 2000000 | 0.8086 ± 0.0051 | 4775 ± 94 | 15.51 ± 0.10 |
| 1500000 | 0.7632 ± 0.0049 | 3762 ± 76 | 14.65 ± 0.09 |
| 1000000 | 0.7430 ± 0.0043 | 2610 ± 53 | 14.28 ± 0.08 |
| 500000 | 0.7004 ± 0.0039 | 1372 ± 28 | 13.47 ± 0.07 |
| 200000 | 0.6633 ± 0.0035 | 665.7 ± 13.5 | 12.77 ± 0.07 |
| 100000 | 0.6467 ± 0.0033 | 361.2 ± 7.3 | 12.45 ± 0.06 |
| 50000 | 0.6283 ± 0.0031 | 209.3 ± 4.2 | 12.10 ± 0.06 |
| 20000 | 0.5937 ± 0.0028 | 97.9 ± 2.0 | 11.43 ± 0.05 |
| 10000 | 0.5439 ± 0.0024 | 57.6 ± 1.2 | 10.47 ± 0.05 |
| 5000 | 0.4888 ± 0.0020 | 37.7 ± 0.8 | 9.41 ± 0.04 |
| 2000 | 0.4269 ± 0.0015 | 24.0 ± 0.5 | 8.22 ± 0.03 |
| 1000 | 0.3667 ± 0.0012 | 18.2 ± 0.4 | 7.06 ± 0.02 |
| 500 | 0.3415 ± 0.0010 | 14.4 ± 0.3 | 6.58 ± 0.02 |
| 200 | 0.3131 ± 0.0009 | 11.1 ± 0.2 | 6.03 ± 0.02 |
| 100 | 0.2915 ± 0.0008 | 9.2 ± 0.2 | 5.62 ± 0.01 |
| 50 | 0.2627 ± 0.0006 | 6.7 ± 0.1 | 5.06 ± 0.01 |

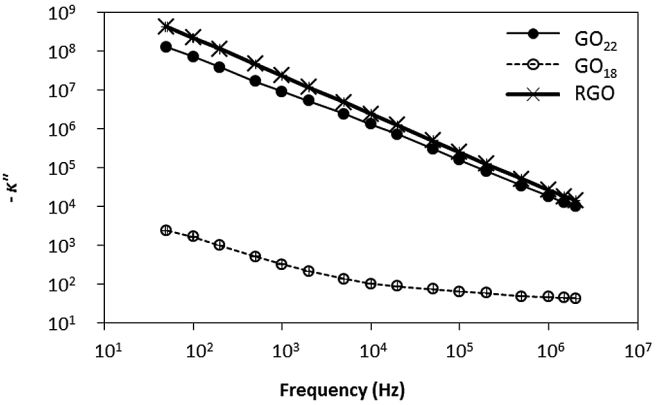


**Fig. 10.** The negative of the imaginary part of the relative dielectric constant vs. the frequency for the non-air part of the $GO_{18}$/$GO_{22}$/RGO paper. The results for the $GO_{18}$ paper is not as reliable, due to the relatively low conductivity of this material and the use of Eq. (24).

effective conductivity increases with increasing frequency. It is attributed to a type of interaction between the sorbed water molecules and the functional groups of the GO, such that the interaction intensifies with increasing frequency. This interaction may relate to the interaction (presently unclear) that is responsible for the large negative values of the calculated effective relative dielectric constant (real part) of the additional sorbed water in Table 2. However, the inadequacy of the Rule of Mixtures may have contributed to causing these extraordinary values of the effective conductivity.

Fig. 9(b) shows that the interfacial resistivity for the interface of the non-air part with the electrical contact is lower for $GO_{22}$ than $GO_{18}$. This is inconsistent with the previous report (based on impedance spectroscopy) that the interfacial impedance increases with increasing humidity [1]. This inconsistency is attributed to the issue with impedance spectroscopy, as explained in Sec. 1. The finding of this work means that the presence of additional sorbed water in the $GO_{22}$ paper improves the quality of the electrical contact. Furthermore, the interfacial resistivity decreases with increasing frequency, such that the decrease is more precipitous for $GO_{18}$ than $GO_{22}$. This reflects that sorbed water remains quite conductive as the frequency increases.

At any of the frequencies studied, the interfacial resistivity is much higher for $GO_{22}$ than RGO [14] (Fig. 9(b) and Table 4). This reflects the lower conductivity of $GO_{22}$ compared to RGO. This also suggests that, in spite of the ionic conductivity of the water, the presence of water at the interface of the electrical contact with $GO_{22}$ is not enough for decreasing the interfacial resistivity to the level of RGO. This in turn suggests the important role of electronic conduction (as opposed to ionic conduction) in $GO_{22}$.)

Fig. 9(c) shows that the ratio of the through-thickness conductivity of the non-air part of the $GO_{22}$ paper to that of the $GO_{18}$ paper decreases with increasing frequency. The highest value of this ratio is 40,000 (which occurs at the lowest frequency of 50 Hz), indicating that the through-thickness conductivity is much higher for the $GO_{22}$ paper than the $GO_{18}$ paper, as expected. At frequencies above 1 MHz, the ratio is about 200. These results mean that the effect of sorbed water on the conductivity decreases with increasing frequency.

Fig. 10 shows that the negative of the imaginary part of the relative dielectric constant is higher for the non-air part of the $GO_{22}$ paper than that of the $GO_{18}$ paper, as expected due to the higher conductivity of the $GO_{22}$ paper. The value decreases with increasing frequency (as expected from Eq. (23)), such that the decrease is more precipitous for the $GO_{22}$ paper than the $GO_{18}$ paper. In Fig. 10, the values are reliable for the $GO_{22}$ paper. However, due to the relatively low conductivity of the $GO_{18}$ paper, the values are not reliable for the $GO_{18}$ paper.

For the $GO_{22}$, the value of the negative of the imaginary part of the relative dielectric constant ranges from $10^4$ to $10^8$. The values in this range are high compared to a previously reported value of essentially zero when an insulating film is used during the measurement [9] and a previously reported value ranging from 10 to $10^3$ when an insulating film is not used [9]. A discussion of the issues with the previously reported values is in Sec. 1.2.

At any of the frequencies studied, the negative of the imaginary part of the relative dielectric constant is lower for $GO_{22}$ than RGO (Fig. 10). This reflects the lower conductivity of the former (Fig. 9(a)).

Fig. 11(a) shows that the dielectric loss angle $\delta$ is higher for the non-air part of the $GO_{22}$ paper than that of the $GO_{18}$ paper, as expected, due to the higher conductivity of the former. For the $GO_{22}$ paper, the angle is essentially at the maximum value of 90° for all frequencies. For the $GO_{18}$ paper, the angle decreases with increasing frequency, as expected from Eq. (25). However, due to the relatively low conductivity of the $GO_{18}$ paper, the values for the loss angle are not reliable for the $GO_{18}$ paper.

The dielectric loss angle is close at low frequencies (<50 kHz) for $GO_{22}$ and RGO, but it is higher for $GO_{22}$ than RGO at high frequencies (>50 kHz) (Fig. 11(b)). The tangent of this angle relates to the ratio of the conductivity to the relative dielectric constant (real

**Table 4**
Comparison of the electrical and dielectric properties of $GO_{18}$ [13], $GO_{22}$ (this work) and RGO [14]. The properties are all for the non-air part of the corresponding paper. Each entry gives the range of values from the value at 50 Hz (first value shown in the range) to the value at 2 MHz (second value shown in the range). $\sigma_\perp$ = through-thickness conductivity; $\sigma_{//}$= in-plane conductivity; $\rho_i$ = interfacial resistivity; $C_c$ = specific interfacial capacitance.

| | $GO_{18}$ [13] | $GO_{22}$ (this work) | RGO [14] |
|---|---|---|---|
| $\sigma_\perp$ (S/m) | $6.7 \times 10^{-6}$–$4.8 \times 10^{-3}$ | 0.35–1.09 | 1.17–1.61 |
| $\sigma_{//}$(S/m) | 0.081–2.35 | 13.7–35.0 | 22.1–114.0 |
| $\sigma_{//}/\sigma_\perp$ | 12135–492 | 38.8–32.1 | 18.96–70.87 |
| $\kappa'$ | 914.6–91.2 | 1504–47 | 1128–206 |
| $-\kappa''$ | $2.4 \times 10^3$–$4.3 \times 10^1$ | $1.3 \times 10^9$–$9.8 \times 10^3$ | $4.2 \times 10^8$–$1.4 \times 10^4$ |
| $\rho_i$ (Ω.cm$^2$) | $1.5 \times 10^5$–$1.0 \times 10^2$ | 79.6–15.2 | 0.1764–0.1699 |
| $C_c$ (μF/m$^2$) | 18.33–1.11 | 39.74–0.52 | 0.3085–0.2239 |

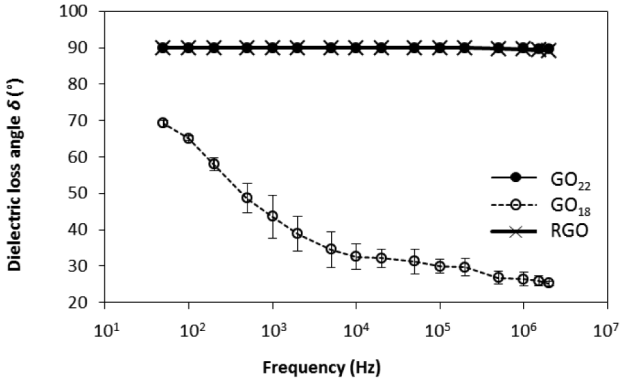


(a)

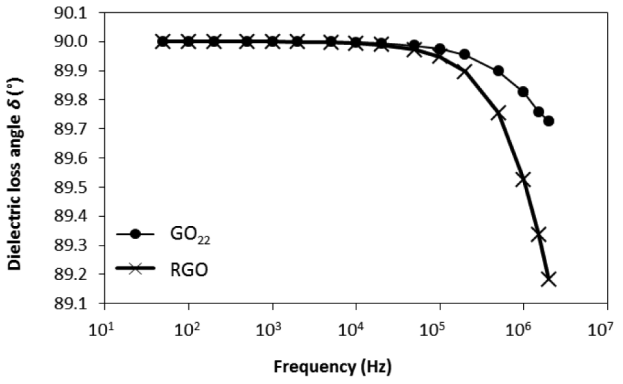


(b)

**Fig. 11.** The dielectric loss angle $\delta$ vs. the frequency for the non-air part of the $GO_{18}$/$GO_{22}$/RGO paper. The results for the $GO_{18}$ paper is not as reliable, due to the relatively low conductivity of this material and the use of Eq. (24). (a) All three materials shown using a coarse vertical scale, with the data for $GO_{22}$ and RGO overlapping. (b) Only $GO_{22}$ and RGO shown, using a fine vertical scale.

part) (Eq. (24)). This difference between $GO_{22}$ and RGO in the high-frequency regime is consistent with the fact that both the conductivity and the relative dielectric constant (real part) are lower for $GO_{22}$ compared to RGO.

### 3.4. In-plane electrical conductivity

Fig. 12(a) shows the in-plane conductivity of the non-air part of the $GO_{22}$ paper of three different thicknesses. Fig. 12(b) shows that, at any of the frequencies studied, RGO exhibits higher in-plane conductivity than $GO_{22}$, which in turn exhibits much higher in-plane conductivity than $GO_{18}$. The high in-plane conductivity of $GO_{22}$ compared to $GO_{18}$ [13] is expected, due to the conductivity of the additional sorbed water in $GO_{22}$. The fact that the in-plane conductivity is higher for RGO than $GO_{22}$ indicates that the conductivity of the sorbed water is not enough for $GO_{22}$ to be as conductive as RGO. Such difference between RGO and $GO_{22}$ similarly applies to the through-thickness conductivity (Fig. 9(a)).

The in-plane conductivity of the $GO_{22}$ paper decreases slightly with increasing thickness, due to the expected increase in the degree of preferred orientation of the carbon layers with decreasing thickness. The trend is the same for the $GO_{18}$ paper [13], but the effect of the thickness is smaller for the $GO_{18}$ paper than the $GO_{22}$ paper. The more severe dependence on the thickness for the $GO_{22}$ paper is probably due to the additional sorbed water inhibiting the preferred orientation of the carbon layers.

Fig. 12(c) shows that the ratio of the in-plane conductivity of $GO_{22}$ to that of $GO_{18}$ decreases with increasing frequency, with the highest value of 170 occurring at the lowest frequency of 50 Hz. The ratio is much smaller than the corresponding ratio for the through-thickness conductivity (Fig. 9(c)). This indicates that the additional sorbed water influences the through-thickness conductivity much more than the in-plane conductivity.

At any of the frequencies (50 Hz–2 MHz), the in-plane conductivity of $GO_{22}$ is lower than that of RGO (13.7–35.0 S/m for $GO_{22}$, compared to 22.1–114 S/m for RGO) (Table 4, Fig. 12(b)).

The ratio of the in-plane conductivity of $GO_{22}$ to RGO (both being the non-air part) is less than 1 for all the frequencies, such that it increases with increasing frequency at frequencies up to 50 kHz and decreases precipitously above 50 kHz (Fig. 12(d)). The in-plane conductivity increases with increasing frequency for both $GO_{22}$ and RGO [14], but the increase is more significant for the former in the low frequency regime. This is probably due to the difference in defects and sorbed water content between $GO_{22}$ and RGO. The defects and sorbed water interfere the electron excursion in a cycle, and the excursion decreases as the frequency increases. The increase of this ratio with increasing frequency up to 50 kHz is attributed to the more significant increase of the conductivity with increasing frequency for $GO_{22}$ than RGO [14]. The precipitous decrease of the ratio above 50 kHz is attributed to the abrupt increase in the conductivity of RGO at high frequencies [14].

### 3.5. Conductivity anisotropy

Fig. 13 shows that the ratio of the in-plane conductivity to the through-thickness conductivity is lower for the $GO_{22}$ paper than the $GO_{18}$ paper. In other words, the $GO_{18}$ paper is more anisotropic than the $GO_{22}$ paper. This is expected, due to fact that the anisotropy is mainly derived from the carbon layers rather than the sorbed water, which may hinder the preferred orientation. The degree of anisotropy decreases with increasing frequency for the $GO_{18}$ paper, but is relatively independent of the frequency for the $GO_{22}$ paper.

The ratio of the in-plane conductivity to through-thickness conductivity is comparable for $GO_{22}$ and RGO (Fig. 13). The ratio is higher for $GO_{22}$ than RGO at up to 0.5 MHz and is lower for $GO_{22}$ than RGO above 0.5 MHz. This means that $GO_{22}$ is more anisotropic than RGO below 0.5 MHz, but is less anisotropic than RGO above 0.5 MHz. This difference between $GO_{22}$ and RGO is attributed to the difference in defect and sorbed water contents and the interference of the defects and sorbed water to the electron excursion.

Fig. 14(a) shows that the interfacial contribution to the measured capacitance is much larger than the volumetric contribution for all three thicknesses of the $GO_{22}$. In contrast, Fig. 14(b) shows that the interfacial contribution to the measured resistance is much smaller than the volumetric contribution for all three thicknesses of the $GO_{22}$. In both Fig. 14(a) and (b), the larger is the thickness, the smaller is the interfacial contribution proportion, as expected. Both the high proportion of the interfacial capacitance and the low proportion of the interfacial resistance indicate that the interface does not influence the measured capacitance or resistance greatly.

Fig. 15(a) shows that the interfacial capacitance proportion is higher for $GO_{18}$ than $GO_{22}$, and is higher for $GO_{22}$ than RGO. Fig. 15(b) shows that the interfacial resistance proportion is much lower for $GO_{22}$ than RGO, and is lower for RGO than $GO_{18}$. This means that the additional sorbed water in $GO_{22}$ decreases both interfacial capacitance proportion and interfacial resistance

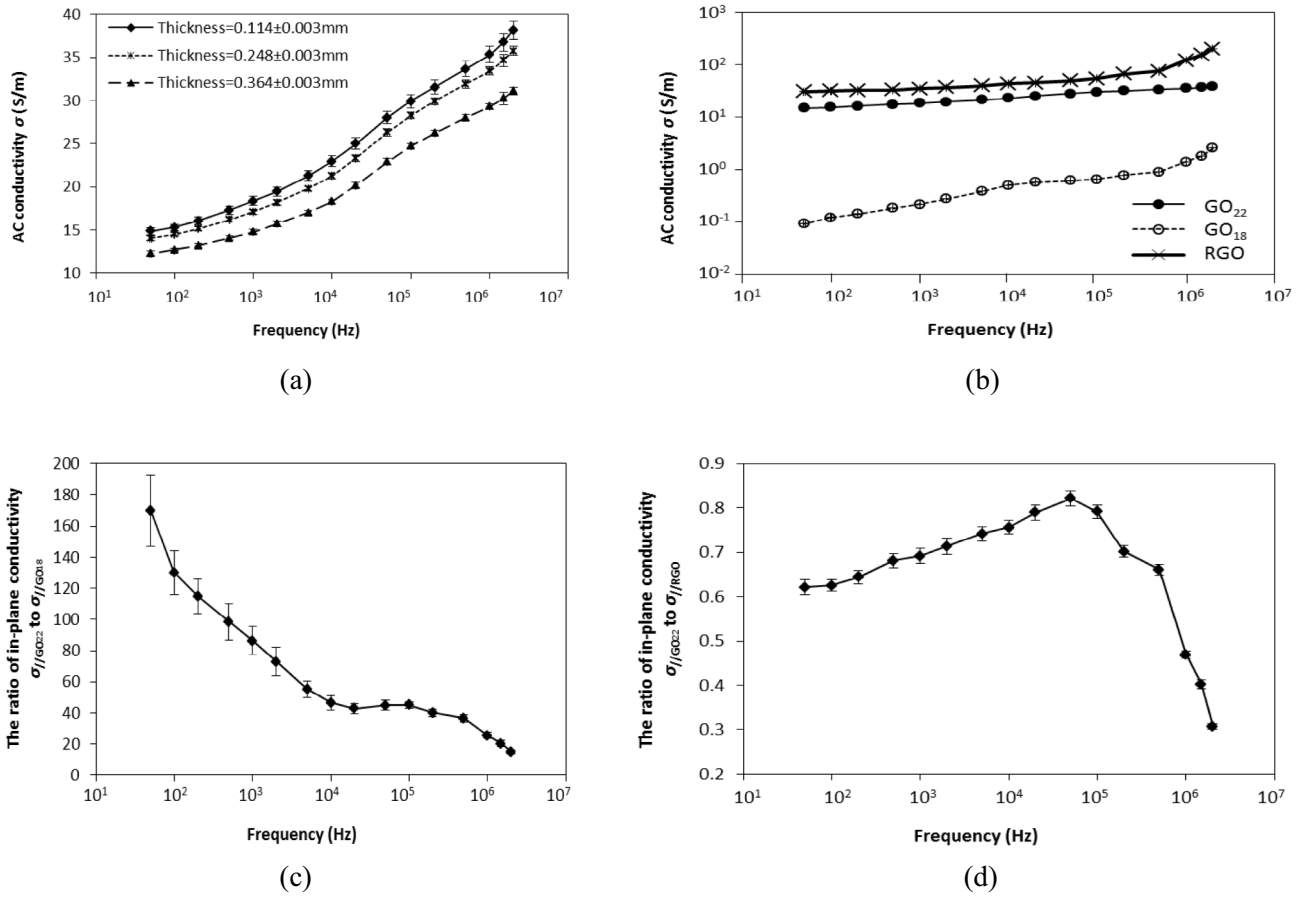


**Fig. 12.** (a) The in-plane electrical conductivity of the non-air part vs. the frequency for three thicknesses of the $GO_{22}$ paper. (b) The in-plane conductivity of the non-air part of the $GO_{18}/GO_{22}$/RGO paper at similar thicknesses in the range from 0.100 to 0.114 mm. (c) The ratio of the in-plane conductivity $\sigma_{//GO22}$ of the non-air part of the $GO_{22}$ paper to that $\sigma_{//GO18}$ of the $GO_{18}$ paper vs. the frequency. (d) The ratio of the in-plane conductivity $\sigma_{//GO22}$ of the non-air part of the $GO_{22}$ paper to that $\sigma_{//RGO}$ of the RGO paper vs. the frequency.

proportion, probably due to the presence of water at the interface. The RGO gives the lowest interfacial capacitance proportion and much higher interfacial resistance proportion than $GO_{22}$. This means that the interface for RGO influences the measured capacitance or resistance more than $GO_{22}$, due to the absence of water at the interface.

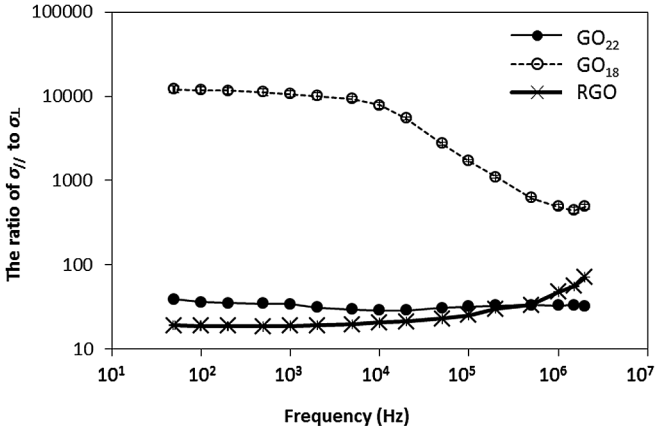


**Fig. 13.** The ratio of the in-plane conductivity to the through-thickness conductivity vs. the frequency for the non-air part of the $GO_{22}/GO_{18}$/RGO paper.

## 4. Conclusions

This paper reports the unexpectedly strong effect of merely 4 wt % additional sorbed water on the electrical and dielectric properties of GO containing 18 wt% sorbed water. That the through-thickness permittivity of GO paper with a higher water content may be modeled electrically as three components (GO at a lower water content, additional sorbed water beyond that corresponding to the lower water content, and air) in parallel is also unexpected, due to the preferred orientation of the carbon layers in the in-plane direction.

This paper provides rich information that encompasses volumetric and interfacial properties at frequencies ranging from 50 Hz to 2 MHz and includes the relative dielectric constant, conductivity, interfacial resistivity and specific interfacial capacitance in the through-thickness direction, and the in-plane conductivity. The comprehensiveness and quantitativeness of the information are above that of the prior work. Moreover, this paper provides a comparison with the prior work, as necessitated by the differences in experimental methods. In addition, this paper provides a comparison of $GO_{22}$ with RGO in terms of the electrical and dielectric properties.

The sorbed water contents of $GO_{18}$ (as obtained by heating at 60 °C for 3 h immediately before testing) and $GO_{22}$ (without this heating) are 17.9 and 21.8 wt% respectively, corresponding to $C/H_2O$ (total sorbed water) mole ratio of 4.5 and 3.7 respectively, i.e., 44%

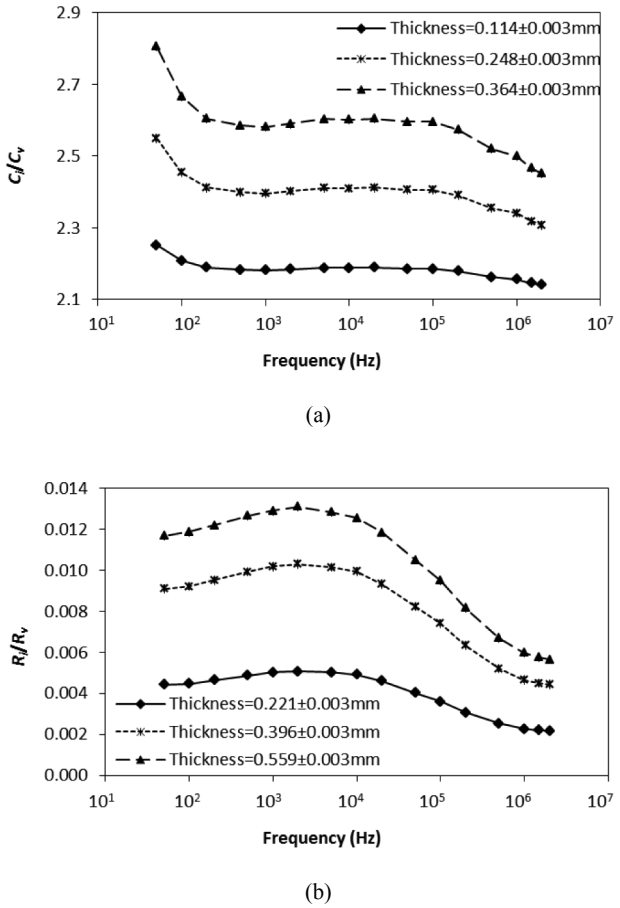


**Fig. 14.** Ratio of the interfacial contribution to the volumetric contribution for the through-thickness capacitance/resistance of the non-air part of the $GO_{22}$ paper. Data for three thicknesses are shown. (a) Contribution to the measured capacitance. (b) Contribution to the measured resistance.

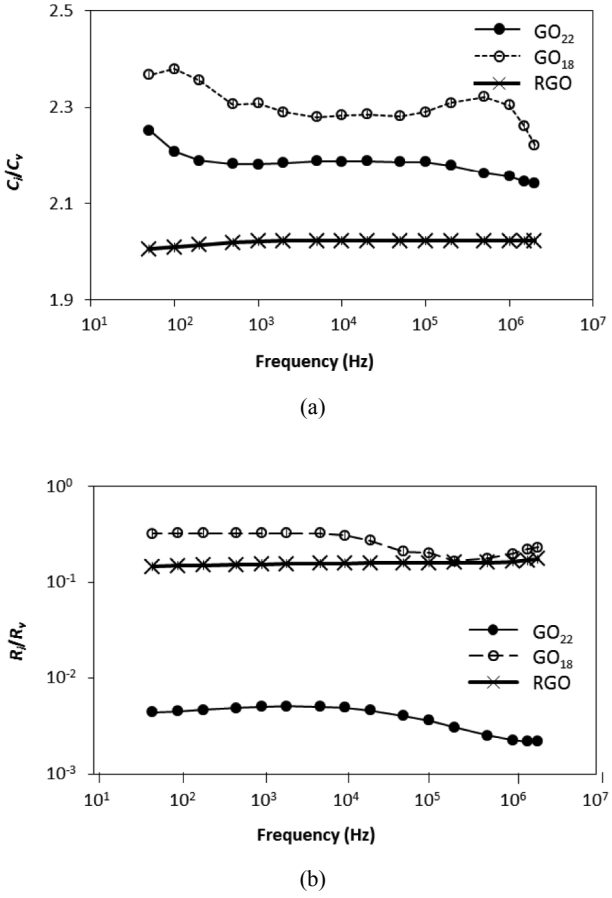


**Fig. 15.** Ratio of the interfacial contribution to the volumetric contribution for the through-thickness capacitance/resistance of the non-air part of the $GO_{22}/GO_{18}/RGO$ paper. The thicknesses are in the range from 0.100 to 0.114 mm for all three materials. (a) Contribution to the measured capacitance. (b) Contribution to the measured resistance.

and 53% of the oxygen atoms correspond to a water molecule, respectively. The difference in sorbed water content (~3.3 wt%) is not large. This extra amount of sorbed water that is present in $GO_{22}$ is in addition to the amount of sorbed water present in $GO_{18}$. In spite of its small amount, the additional sorbed water has profound effects on the electrical and dielectric properties.

Due to the additional sorbed water in $GO_{22}$, the through-thickness conductivity is increased by 2–5 orders of magnitude (depending on the frequency), while the in-plane conductivity is increased by 1–2 orders. RGO exhibits higher through-thickness or in-plane conductivity than $GO_{22}$, which in turn exhibits much higher through-thickness or in-plane conductivity than $GO_{18}$.

For GO, the ratio of the in-plane conductivity to through-thickness conductivity is decreased by the additional sorbed water by 1–3 orders of magnitude. In other words, the additional sorbed water increases the conductivity (particularly the through-thickness conductivity) and decreases the conductivity anisotropy. The relative dielectric constant (real part) of GO is increased by the additional sorbed water at low frequencies (<200 Hz), but is decreased at high frequencies. Thus, the additional sorbed water enhances the conductivity at any of the frequencies, but enhances the polarization ability only at low frequencies (<200 Hz).

At high frequencies (>200 Hz), the relative dielectric constant (real part) is lower for $GO_{22}$ than $GO_{18}$, suggesting that the additional sorbed water in $GO_{22}$ contributes to inhibiting the excursion of the electrons in the GO during polarization at frequencies at which the water molecules are not able to contribute to the polarization. The difference in dielectric constant between $GO_{22}$ and $GO_{18}$ decreases with increasing frequency above 1 kHz. The values are close at frequencies above 0.1 MHz, due to the small distance of excursion of the electrons at high frequencies and the consequent reduced inhibiting influence of the additional sorbed water to the excursion.

The through-thickness relative dielectric constant (real part) and through-thickness conductivity of $GO_{22}$ are modeled by using the Rule of Mixtures, with the three constituents ($GO_{18}$, additional sorbed water and air) in parallel electrically in the through-thickness direction. The model overestimates the relative dielectric constant of $GO_{22}$ at frequencies $\geq$200 Hz, due to the fact that the relative dielectric constant of water at high frequencies is actually less that the assumed value of 80. The model underestimates at frequencies $\leq$100 Hz, probably due to the unaccounted interaction between the additional sorbed water molecules and the functional groups on the GO. However, at 100–200 Hz, the model agrees quite well with the measured values.

The model suggests that the effective relative dielectric constant and effective conductivity of the additional sorbed water are extraordinarily high. This in turn suggests considerable interaction between the sorbed water and the GO. However, the inadequacy of

the Rule of Mixtures may have contributed to causing these extraordinary values.

Concerning the specimen-contact interface, the interfacial resistivity is decreased by the additional sorbed water, due to the ionic conductivity of water. However, the specific interfacial capacitance is decreased, presumably due to the increased thickness of the water at this interface.

Compared to RGO [14], $GO_{22}$ exhibits lower conductivity (both through-thickness and in-plane), higher interfacial resistivity and higher specific interfacial capacitance, indicating that the sorbed water in $GO_{22}$ is not as effective as reduction of the GO to form RGO for increasing the conductivity and decreasing the interfacial resistivity. The relative dielectric constant (real part) of $GO_{22}$ is higher than that of RGO at low frequencies, but is lower than that of RGO at high frequencies.

For $GO_{22}$, the interfacial contribution to the measured capacitance is much larger than the volumetric contribution, while the interfacial contribution to the measured resistance is much smaller than the volumetric contribution. This indicates that the interface does not influence the measured capacitance or resistance greatly. The interfacial capacitance proportion is higher for $GO_{18}$ than $GO_{22}$, and is higher for $GO_{22}$ than RGO. The interfacial resistance proportion is much lower for $GO_{22}$ than RGO, and is lower for RGO than $GO_{18}$.

This paper also provides clarification of the results of related prior work [9,11], in addition to providing explanation of the issues associated with the experimental methods of the prior work. The issues concern (i) the assumption that the electrical parameters are independent of the frequency in the analysis used in impedance spectroscopy [11], (ii) the inappropriate use of an RLC meter to measure the impedance of a conductive material [9], and (iii) the inadequate decoupling of the volumetric and interfacial contributions to the measured capacitance/resistance [9,11]. The values of the relative dielectric constant (real part) reported here are much higher than those previously reported based on impedance spectroscopy [11]. The values of the relative dielectric constant (imaginary part) are much higher than those previously reported based on an inappropriate use of an RLC meter [9].

## References


[1] Y. Yao, X. Chen, J. Zhu, B. Zeng, Z. Wu, X. Li, The effect of ambient humidity on the electrical properties of graphene oxide films, Nanoscale Research Lett. 7 (1) (2012) 1.

[2] Zhao C, Qin M, Huang Q. Humidity sensing properties of the sensor based on graphene oxide films with different dispersion concentrations. SENSORS, 2011 IEEE Conference, http://dx.doi.org/10.1109/icsens.2011.6126968.

[3] R.R. Nair, H.A. Wu, P.N. Jayaram, I.V. Grigorieva, A.K. Geim, Unimpeded permeation of water through helium-leak-tight graphene-based membranes, Science 335 (6067) (2012) 442–444.

[4] S. Borini, R. White, D. Wei, M. Astley, S. Haque, E. Spigone, N. Harris, J. Kivioja, T. Ryhänen, Ultrafast graphene oxide humidity sensors, ACS Nano 7 (12) (2013) 11166–11173.

[5] Y. Zhu, S. Murali, W. Cai, X. Li, J.W. Suk, J.R. Potts, R.S. Ruoff, Graphene and graphene oxide: synthesis, properties, and applications, Adv. Mater 22 (2010) 3906–3924.

[6] G. Eda, M. Chhowalla, Chemically derived graphene oxide: towards large-area thin-film electronics and optoelectronics, Adv. Mater 22 (2010) 2392–2415.

[7] S. Rani, D. Kumar, M. Kumar, Improvement in humidity sensing of graphene oxide by amide functionalization, Sensors Transducers 193 (10) (2015) 100–105.

[8] A. Lerf, A. Buchsteiner, J. Pieper, S. Schottl, I. Dekany, T. Szabo, H.P. Boehm, Hydration behavior and dynamics of water molecules in graphite oxide, J. Phys. Chem. Solids 67 (2006) 1106–1110.

[9] J. Yu, Y. Tian, M. Gu, T.B. Tang, Anomalous dielectric relaxation of water confined in graphite oxide, J. Appl. Phys. 118 (2015) 124104.

[10] V.A. Smirnov, N.N. Denisov, A.E. Ukshe, Y.M. Shul'ga, Effect of humidity on the conductivity of graphite oxide during its photoreduction, High. Energy Chem. 47 (5) (2013) 242–246.

[11] T. Bayer, S.R. Bishop, N.H. Perry, K. Sasaki, S.M. Lyth, Tunable mixed ionic/electronic conductivity and permittivity of graphene oxide paper for electrochemical energy conversion, ACS Appl. Mater. Interfaces 8 (2016) 11466–11475.

[12] W. Gao, N. Singh, Li Song, Z. Liu, A.L.M. Reddy, L. Ci, R. Vajtai, Q. Zhang, B. Wei, P.M. Ajayan, Direct laser writing of micro-supercapacitors on hydrated graphite oxide films, Nat. Nanotech 6 (8) (2011) 496–500.

[13] X. Hong, W. Yu, A. Wang, D.D.L. Chung, Graphite oxide paper as a polarizable electrical conductor in the through-thickness direction, Carbon 109 (2016) 874–882.

[14] X. Hong, W. Yu, D.D.L. Chung, Electric permittivity of reduced graphite oxide, Carbon 111 (2017) 182–190.

[15] X. Hong, D.D.L. Chung, Exfoliated graphite with relative dielectric constant reaching 360, obtained by exfoliation of acid-intercalated graphite flakes without subsequent removal of the residual acidity, Carbon 91 (2015) 1–10.

[16] A. Wang, D.D.L. Chung, Dielectric and electrical conduction behavior of carbon paste electrochemical electrodes, with decoupling of carbon, electrolyte and interface contributions, Carbon 72 (2014) 135–151.

[17] D.D.L. Chung, A review of exfoliated graphite, J. Mater Sci. 51 (1) (2016) 554–568.

[18] W.S. Hummers Jr., R.E. Offeman, Preparation of graphitic oxide, J. Am. Chem. Soc. 80 (6) (1958), 1339–1339.

[19] H. Shin, K.K. Kim, A. Benayad, S. Yoon, H.K. Park, I. Jung, M.H. Jin, H. Jeong, J.M. Kim, J. Choi, Y.H. Lee, Efficient reduction of graphite oxide by sodium borohydride and its effect on electrical conductance, Adv. Funct. Mater 19 (12) (2009) 1987–1992.

[20] S. Mayavan, J. Sim, S.M. Choi, Simultaneous reduction, exfoliation and functionalization of graphite oxide into graphene-platinum nanoparticles hybrid toward methanol oxidation, J. Mater Chem. (22) (2012) 6953–6958. Supporting Information, http://www.rsc.org/suppdata/jm/c2/c2jm15566d/c2jm15566d.pdf. as viewed on Aug. 1, 2016.

[21] S. Tankovich, D.A. Dikin, R.D. Piner, K.A. Kohlhaas, A. Kleinhammes, Y. Jia, R.S. Ruoff, Synthesis of graphene-based nanosheets via chemical reduction of exfoliated graphite oxide, Carbon 45 (7) (2007) 1558–1565.

[22] C. Bao, L. Song, C.A. Wilkie, B. Yuan, Y. Guo, Y. Hu, X. Gong, Graphite oxide, graphene, and metal-loaded graphene for fire safety applications of polystyrene, J. Mater Chem. 22 (2012) 16399–16406.

[23] H. Jeong, Y.P. Lee, R.J.W.E. Lahaye, M. Park, K.H. An, I.J. Kim, C. Yang, C.Y. Park, R.S. Ruoff, Y.H. Lee, Evidence of graphitic AB stacking order of graphite oxides, J. Am. Chem. Soc. 130 (4) (2008) 1362–1366.

[24] S. Cerveny, F. Barroso-Bujans, A. Alegria, J. Colmenero, Dynamics of water intercalated in graphite oxide, J. Phys. Chem. C 114 (2010) 2604–2612.

[25] J. Boguslawski, J. Sotor, G. Sobon, R. Kozinski, K. Librant, M. Aksienionek, L. Lipinska, K.M. Abramski, Graphene oxide paper as a saturable absorber for Er- and Tm-doped fiber lasers, Photonics Res. 3 (4) (2015) 119–124.

[26] Y. Takizawa, D.D.L. Chung, Through-thickness thermal conduction in glass fiber polymer-matrix composites and its enhancement by composite modification, J. Mater Sci. 51 (2016) 3463–3480.